

See discussions, stats, and author profiles for this publication at: <https://www.researchgate.net/publication/234891150>

Vibrational spectra and intramolecular vibrational redistribution in highly excited deuterobromochlorofluoromethane CDBrClF: Experiment and theory

ARTICLE in THE JOURNAL OF CHEMICAL PHYSICS · AUGUST 2000

Impact Factor: 2.95 · DOI: 10.1063/1.1302083

CITATIONS

25

READS

6

5 AUTHORS, INCLUDING:



Jürgen Stohner

Zurich University of Applied Sciences

37 PUBLICATIONS 785 CITATIONS

SEE PROFILE

Vibrational spectra and intramolecular vibrational redistribution in highly excited deuterobromochlorofluoromethane CDBrClF: Experiment and theory

Andreas Beil, Hans Hollenstein, Oliver L. A. Monti, Martin Quack, and Jürgen Stohner

Citation: *J. Chem. Phys.* **113**, 2701 (2000); doi: 10.1063/1.1302083

View online: <http://dx.doi.org/10.1063/1.1302083>

View Table of Contents: <http://jcp.aip.org/resource/1/JCPSA6/v113/i7>

Published by the AIP Publishing LLC.

Additional information on J. Chem. Phys.

Journal Homepage: <http://jcp.aip.org/>


Journal Information: http://jcp.aip.org/about/about_the_journal

Top downloads: http://jcp.aip.org/features/most_downloaded

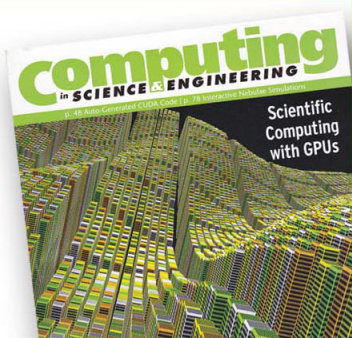
Information for Authors: <http://jcp.aip.org/authors>

ADVERTISEMENT

**SHARPEN YOUR
COMPUTATIONAL
SKILLS.**



Subscribe for
\$49 | year



computing
in **SCIENCE & ENGINEERING**

Scientific
Computing
with GPUs

Vibrational spectra and intramolecular vibrational redistribution in highly excited deuterobromochlorofluoromethane CDBrClF: Experiment and theory

Andreas Beil,^{a)} Hans Hollenstein, Oliver L. A. Monti,^{b)} Martin Quack,^{c)} and Jürgen Stohner

Laboratorium für Physikalische Chemie, ETH-Zürich (Zentrum), 8092 Zürich, Switzerland

(Received 12 August 1999; accepted 3 December 1999)

The rovibrational spectra of deuterobromochlorofluoromethane (CDBrClF) were measured at intermediate (0.1 cm^{-1}) and high resolution (0.0024 cm^{-1} full bandwidth, half-maximum) by interferometric Fourier transform infrared spectroscopy in the range from the far infrared at 200 cm^{-1} to the near infrared ($12\,000\text{ cm}^{-1}$) covering all the fundamentals and CD stretching overtones up to polyad $N=5$. The spectra are completely analyzed in terms of their vibrational assignments to fundamentals, combinations and overtones. At high excitation the analysis reveals the dominant anharmonic coupling between four high frequency vibrational modes; the CD stretching (ν_1), two CD bending (ν_2, ν_3), and the CF stretching mode (ν_4). The analysis is carried out using effective model Hamiltonians including three and four vibrational degrees of freedom. We also present vibrational variational calculations on a grid in a four-dimensional normal coordinate subspace. The potential energy and the dipole moment function are calculated *ab initio* on this grid using self-consistent field second order Møller–Plesset perturbation theory (MP2). Experimental and theoretical results for band positions and integrated intensities as well as effective spectroscopic parameters are found to be in good agreement. The important anharmonic coupling between the CD chromophore and the CF stretching vibration can be described by an effective cubic Fermi resonance coupling constant $k'_{sff} \approx (50 \pm 10)\text{ cm}^{-1}$, which leads to intramolecular vibrational redistribution between the CD and CF chromophores on the femtosecond time scale. Time dependent intramolecular vibrational redistribution processes in CDBrClF are derived in various representations, including time dependent probability densities (“wave packets”) in coordinate space and finally time dependent entropy. © 2000 American Institute of Physics. [S0021-9606(00)02008-0]

I. INTRODUCTION

Understanding intramolecular dynamics is of crucial importance for the investigation of unimolecular reaction dynamics and laser chemistry.^{1–10} Rovibrational and intramolecular vibrational redistribution processes (IVR) have been shown to be particularly important processes in this context.^{3,4} Intramolecular energy transfer on the femtosecond time scale^{5,6} can be derived by the detailed analysis of absorption spectra. The experimental infrared spectra provide a route to a molecular Hamiltonian, and the subsequent solution of the time-dependent Schrödinger equation provides access to the time-dependent intramolecular processes.^{7,8} This approach is attractive because modern high resolution FTIR and laser techniques provide excellent means for measuring rovibrational spectra. However, the route to an adequate approximation to the true molecular Hamiltonian from the experimental spectrum can be very difficult.⁹

One possible approach is to study the main contributions to the Hamiltonian from certain molecular functional groups, to see if dynamical properties are transferable between different molecules and change systematically with the structural environment.¹⁰ Considerable effort has been put into understanding the complex pattern of anharmonic interaction in the overtone region of the CH-/CD-chromophore and subsequent extraction of a vibrational Hamiltonian (for a review on this topic, see, e.g., Ref. 4 and references cited therein). Of particular interest is the CH chromophore in a chiral environment. To this end CHBrClF has been investigated recently in detail.^{11–16} CDBrClF offers the opportunity to study the deuterium isotope effect on IVR in this molecule.

CDBrClF is one of the simplest chiral molecules and has as such been investigated several times together with CHBrClF. However, only studies of the fundamental region^{17,18} with a corresponding Urey–Bradley force field for CHBrClF,¹⁹ vibrational circular dichroism,²⁰ and Raman optical activity²¹ have been reported so far. There does not seem to be much further work on the isotopomer CDBrClF. A detailed literature search did not indicate any other publications beyond those already cited; however, there has been a recent theoretical study of IVR in “CDBrClF” using a highly oversimplified model.²²

^{a)}Present address: Bruker Saxonia Analytik GmbH, FT-IR Abteilung, HPA 5, PF 42, D-04301 Leipzig, Germany.

^{b)}Present address: University of Oxford, Physical and Theoretical Chemistry Laboratory, South Parks Road, Oxford OX1 3QZ, United Kingdom. This is part of a Diploma thesis.

^{c)}Author to whom correspondence should be addressed. Fax: ++41-1-632 10 21; electronic mail: quack@ir.phys.chem.ethz.ch

We report here the complete vibrational spectra of CDBrClF, analyzed from the far infrared range (FIR) to the near infrared range (NIR). The results in the fundamental region are compared to *ab initio* second order Møller–Plesset perturbation theory (MP2) and density functional Becke3–Lee–Yang–Parr (B3LYP) calculations. The experimental overtone spectra are analyzed in terms of effective Hamiltonians involving three and four vibrational degrees of freedom and in terms of vibrational variational calculations on the corresponding *ab initio* potential energy and dipole moment surfaces. We find that the CD chromophore in CD-BrClF is strongly coupled to the CF frame mode which, for the first time, renders such a four-dimensional analysis in an isolated CH(D) chromophore system both necessary and insightful by providing two chiral coupling constants.

II. EXPERIMENT

A. Synthesis of deuterobromochlorofluoromethane

Deuterobromochlorofluoromethane was prepared by decarboxylation of deuterobromochlorofluoroacetic acid in deuterium oxide. The method described by Doyle and Vogl^{23,24} and the alternative route reported by Diem and Burrow¹⁷ with dibromochloromethane gave low yields and insufficient isotopic purity. We therefore modified the synthesis of CDBrClF so as to improve the yields of the decarboxylation step (i.e., 60%) and the isotopic purity (i.e., content in CDBrClF $\geq 99.8\%$). For the preparation of bromochlorofluoroacetic acid we followed the procedure described previously.¹² The precise synthesis procedure is reported in EPAPS.²⁵

The identity of the final product CDBrClF was obvious from the mass spectra (estimated isotopic purity 99.2%) and the infrared absorption spectra (estimated isotopic purity 99.6% from measuring the CH stretching absorption whose band strength is known;¹² thus the latter value is assumed to be more reliable). The chemical purity was estimated to be better than 99.9% as estimated from gas chromatography.

B. Infrared spectroscopy

The spectra were recorded on our BOMEM DA.002 interferometric Fourier transform infrared (FTIR) spectrometer which has been described in detail in Refs. 3, 4, 26. With a maximum optical path difference of 2.5 m it allows for a minimum instrumental bandwidth of 0.0024 cm^{-1} (FWHM of the unapodized line shape function) or 0.004 cm^{-1} (FWHM with Hamming apodization). The whole spectral range from the far infrared (FIR, 200 cm^{-1}) to the near infrared (NIR, $12\,000\text{ cm}^{-1}$) has been covered.

Figure 1 shows a low resolution survey of the well ordered fundamental range, whereas Fig. 2 shows surveys of the high resolution spectra in the important CO₂ laser emission ranges. Spectra covering the complete ranges are summarized in EPAPS.²⁵

We have used as detectors a Si-bolometer in the FIR, CuGe from 350 to 700 cm^{-1} , HgCdTe from 700 to 3000 cm^{-1} , InSb from 2100 to $10\,000\text{ cm}^{-1}$, and a Si-photodiode in the region of 8500 to $12\,000\text{ cm}^{-1}$; as sources a Globalar from 200 to 5000 cm^{-1} and a quartz halogen lamp above

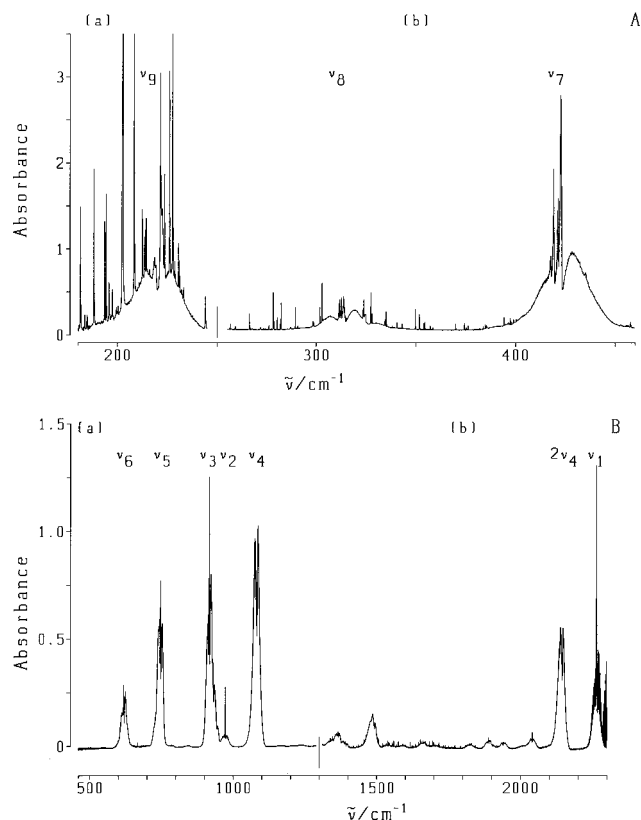


FIG. 1. (a) and (b) Survey spectrum of CDBrClF from 180 to 2300 cm^{-1} [as absorbance $\ln(I_0/I)$, room temperature, resolution 0.1 cm^{-1}]. (A) Far infrared region from 180 to 450 cm^{-1} . Conditions: (a) $l=2100\text{ cm}$, $p=281.8\text{ mbar}$, (b) $l=1400\text{ cm}$, $p=6.3\text{ mbar}$. Traces of water are observed in the lower part of the spectrum. (B) Mid-infrared region from 450 to 2300 cm^{-1} . Conditions: $l=18\text{ cm}$; (a) $p=2.07\text{ mbar}$, (b) $p=72.71\text{ mbar}$. Traces of water, around 1500 cm^{-1} , and of CO₂, near 2300 cm^{-1} , are observed.

5000 cm^{-1} ; as beamsplitters a 3μ - or 6μ -Mylar below 400 cm^{-1} , KBr from 400 to 1500 cm^{-1} , CaF₂ from 1200 to 6000 cm^{-1} , and quartz above 5000 cm^{-1} . Either a short glass cell (path length, 0.18 m) or a multipass glass cell (base length, 1.75 m) equipped with CsI windows from 200 to 600 cm^{-1} , KBr from 400 to 3000 cm^{-1} , and BaF₂ from 1000 to $12\,000\text{ cm}^{-1}$, with nominal path lengths of up to 63 m , were used. Path lengths were determined with the help of a HeNe laser passing through the cell parallel to the source beam. Narrow band optical filters were used where high resolution was required. In case of the Si-bolometer, the CuGe-detector and the InSb-cold window detector, cold optical filters were positioned in front of the detector.

After carefully drying the sample for several hours on P₄O₁₀, thorough degassing by a number of freeze–pump–thaw cycles yielded pure vapor of well defined pressure. The dissolution of large amounts of air and oxygen has been observed to lead in some cases to explosion upon warming up.¹² Cells were filled at a standard vacuum line with pressures ranging from 0.5 mbar to 500 mbar . The pressure was measured with MKS BARATRON pressure gauges calibrated absolutely by MKS Instruments, Inc. and checked by us against Hg manometers.¹² All spectra were recorded at room temperature ($\approx 27^\circ\text{C}$).

Quantitative band strengths in the region of 400 – 2000

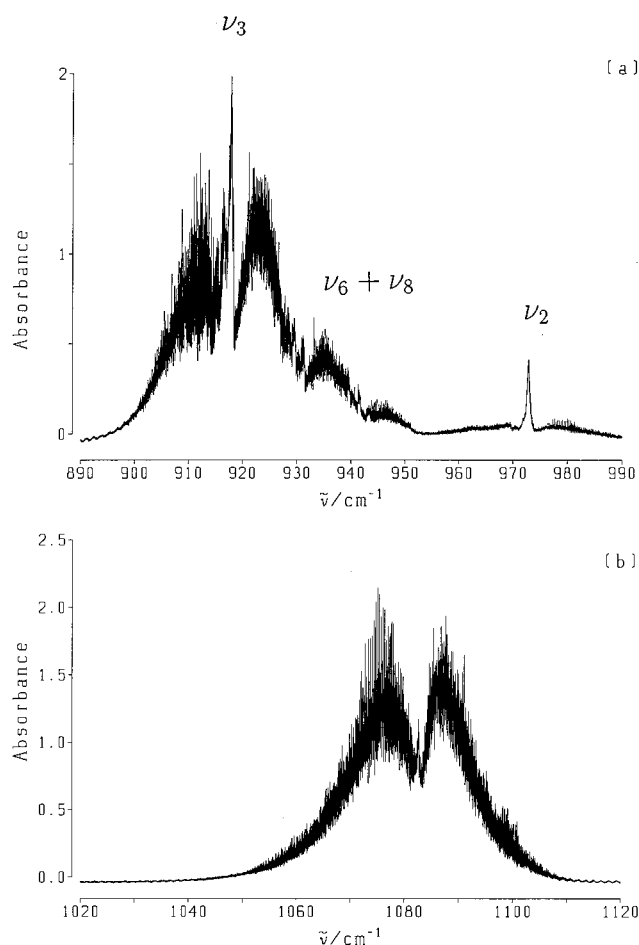


FIG. 2. (a) and (b) High resolution spectra of (a) the CD-bending bands ν_3 and ν_2 and (b) the CF stretching band ν_4 . Conditions: room temperature, resolution 0.0024 cm^{-1} unapodized, $l = 18 \text{ cm}$, $p = 3.12 \text{ mbar}$.

cm^{-1} were measured in pressure broadened spectra (addition of dried nitrogen up to a pressure of 1000 mbar) at a resolution of 0.1 cm^{-1} . The integrated cross section or band strength G_{ji} for a transition from i to j is given by^{4,27,28}

$$G_{ji} = \int_{\text{Band}} \sigma_{ji}(\tilde{\nu}) \tilde{\nu}^{-1} d\tilde{\nu} \quad (1)$$

$$= \frac{8\pi^3}{3hc(4\pi\epsilon_0)} |M_{ji}|^2 \approx 41.6238 \left| \frac{M_{ji}}{D} \right|^2 \text{ pm}^2, \quad (2)$$

with the absorption cross section $\sigma_{ji}(\tilde{\nu})$,

$$\sigma_{ji}(\tilde{\nu}) = C^{-1} l^{-1} \ln \left(\frac{I_0}{I} \right), \quad (3)$$

C is the concentration as particle density, l is the cell length, and $\ln(I_0/I)$ is the absorbance recorded in the spectra. C has been estimated by the ideal gas law from the measured pressures. h is Planck's constant, c the velocity of light, and M_{ji} the transition dipole moment with $|M_{ji}|^2 = \sum_{\rho=x,y,z} |\langle i | \hat{\mu}_\rho | j \rangle|^2$, where $\hat{\mu}_\rho$ is the appropriate component of the electric dipole moment operator.

In the wave number range above 1000 cm^{-1} , stimulated emission can be safely neglected. Below 1000 cm^{-1} the effective observed band strength G_{eff} as measured directly

from $\ln(I_0/I)$ can be converted into an "observed" integrated absorption cross section, G_{obs} , by the following relation:^{12,27}

$$G_{\text{obs}} = G_{\text{eff}} \left[1 - \exp \left(\frac{-hc\tilde{\nu}}{kT} \right) \right]^{-1}, \quad (4)$$

$$G_{\text{eff}} = C^{-1} l^{-1} \int_{\text{Band}} \ln \left(\frac{I_0}{I} \right) \tilde{\nu}^{-1} d\tilde{\nu}, \quad (5)$$

where $\tilde{\nu}$ is the transition wave number, k is the Boltzmann constant, and T is the absolute temperature. The accuracy in the experimental determination of band strengths is estimated to correspond to an uncertainty of 10%–30% although the statistical error is much smaller (<5%).

III. THEORY

A. *Ab initio* calculations of the potential energy and dipole moment surface

Ab initio calculations (MP2) with two basis sets (basis set 1: H:(10s1p)/[6s1p], C:(9s5p1d)/[4s2p1d], F:(9s5p1d)/[4s2p1d], Cl:(12s8p1d)/[6s4p1d], Br:(13s9p5d)/[8s6p2d]; exponents for the polarization functions included $\alpha_p(\text{H})=1.0$, $\alpha_d(\text{C})=0.8$, $\alpha_d(\text{F})=1.2$, $\alpha_d(\text{Cl})=0.75$; otherwise exponents and contraction coefficients as in Refs. 29–31; basis set 2: H:(5s1p)/[3s1p], $\alpha_p(\text{H})=1.0$; C, F, Cl same as in basis set 1; Br: same as in basis set 1 plus (1d1f)/[1d1f], $\alpha_d(\text{Br})=0.54$, $\alpha_f(\text{Br})=0.4$) and density functional calculations (B3LYP, basis set 2) were used to obtain the equilibrium geometry and the harmonic force constants.¹² We used the GAUSSIAN94 (Ref. 32) program including core correlation in the MP2 calculation. The Cartesian representation was used for d functions (6d), the usual polar representation for f functions (7f).

On the basis of a normal mode calculation (MP2, basis set 1), the potential energy and dipole moment surfaces were calculated on a four-dimensional equidistant grid consisting of the four dimensionless reduced rectilinear normal coordinates q_s , q_a , q_b , and q_f associated with the CD stretching (q_s), the two CD bending (q_a, q_b) and the CF stretching (q_f) vibrations. These functions were evaluated in the coordinate ranges ($q_s \in [-6, 10]$, $q_a \in [-8, 8]$, $q_b \in [-8, 8]$, $q_f \in [-10, 6]$) at approximately 15 000 *ab initio* grid points. A spline interpolation scheme was used to adequately represent the surfaces on an interpolated grid of 31 points in each dimension of the four-dimensional reduced normal coordinate subspace. Figure 3 shows graphical representations of the atomic amplitudes for the four coupled normal modes ω_1 , ω_2 , ω_3 , ω_4 ($\omega_s, \omega_a, \omega_b, \omega_f$).

B. Vibrational variational calculations in three and four dimensions

The overtone spectra attributed to the Fermi resonance subspace have been calculated extending the method presented in (Refs. 12, 13, 16) to four dimensions. Thus the model Hamiltonian is given by

$$\hat{H}_m = \frac{1}{2} \sum_{k=s,f,a,b} \omega_k \hat{p}_k^2 + \hat{V}(q_s, q_f, q_a, q_b), \quad (6)$$

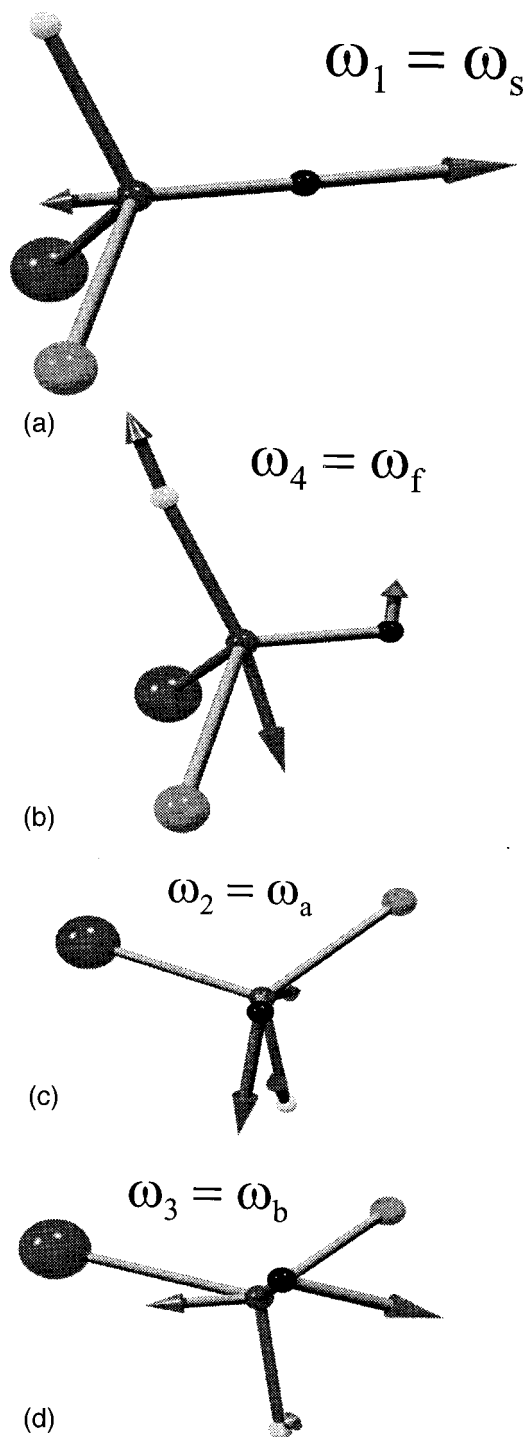


FIG. 3. Atomic displacement vectors of the four highest normal vibrations in CDBrClF (from top to bottom): (a) CD stretching mode (ω_s), (b) CF stretching mode (ω_f), (c) CD bending mode (ω_a , with respect to F-C-D “in-plane”) and (d) CD bending mode (ω_b , with respect to F-C-D “out-of-plane”).

$$q_k = Q_k 2\pi \sqrt{\frac{\omega_k c}{h}}; \quad k \in \{s, f, a, b\}, \quad (7)$$

$$\hat{p}_k = -i \frac{\partial}{\partial q_k}, \quad (8)$$

where q_k is the reduced normal coordinate, \hat{p}_k is the momentum operator conjugate to q_k , ω_k is the corresponding har-

monic wave number, $\hat{V}(q_s, q_f, q_a, q_b)$ is the potential energy operator, and Q_k is the k th normal coordinate. The *ab initio* calculation of the overtone spectra was based on a discrete variable representation (DVR) method formulated by Meyer in one and two dimensions³³ and by Luckhaus and Quack³⁴ in three dimensions together with the adiabatic truncation scheme for the basis as described in detail in Ref. 13. We refer to Refs. 12, 13, 16, 34 for details of the techniques which are not repeated here (see also Refs. 35, 36 for further aspects of related DVR calculations).

C. Anharmonic resonance structure in three and four dimensions

The overtone spectra of CDBrClF were analyzed by means of effective Hamiltonians in three^{3,12,13,37,38} and four dimensions. The three-dimensional effective Hamiltonian $\hat{H}_{\text{eff}}^{3D,F}$ is entirely analogous to Ref. 12 with the following exceptions:

- (1) Instead of the CH stretching and the two CH bending vibrations in CHBrClF the Fermi resonance system is assumed to be due to anharmonic interactions of the CD stretching vibration ν_s , the CF stretching vibration ν_f , and the higher frequency CD bending vibration ν_a . The better fulfillment of the resonance condition by ν_a as compared to ν_b justifies this assumption. Furthermore, the IR spectra show the well known strong CF-chromophore absorptions.³⁹ We have also tried a three-dimensional effective Hamiltonian analysis in the subspace of the three CD normal modes which has however not been able to account even approximately for the observed spectra.
- (2) A quartic effective coupling constant δ' describing the Darling–Dennison resonance between ν_f and ν_a has been introduced. The number of observed band centers did not allow us to determine all possible Darling–Dennison coupling constants between (ν_f, ν_a) , (ν_f, ν_b) , and (ν_a, ν_b) . This has successfully been achieved for the variational data from the 4D *ab initio* potential energy surface, where all variational band centers have been fitted up to about 9000 cm^{-1} (see below).

The analysis within a 3D effective Hamiltonian remains unsatisfactory, since it disregards an important coupling between both CD bending modes. However, the complete vibrational structure of the overtone spectra can be described by a four-dimensional effective Hamiltonian $\hat{H}_{\text{eff}}^{4D}$ in q_s , q_f , q_a , and q_b with polyad quantum number,

$$N = v_s + \frac{1}{2}v_f + \frac{1}{2}v_a + \frac{1}{2}v_b, \quad (9)$$

where v_s , v_f , v_a , and v_b denote the vibrational quantum numbers for the CD stretching (ν_s), CF stretching (ν_f), and the two CD bending (ν_a and ν_b) normal vibrations. The effective Hamiltonian is block-diagonal in the chromophore quantum number N . The diagonal elements,

$$H_{v_s, v_f, v_a, v_b; v_s, v_f, v_a, v_b}^N = \sum_i v_i \bar{v}_i' + \sum_i \sum_{j \geq i} x_{ij}' v_i v_j \quad (10)$$

$$i \in \{s, f, a, b\},$$

are similar to the usual low-order anharmonic term formula with effective vibrational wave numbers $\tilde{\nu}'_i$ and anharmonicities x'_{ij} . The off-diagonal elements describing the Fermi resonances between ν_s and the modes ν_f , ν_a , and ν_b are given by ($i, j \in [a, b, f]$),

$$H_{\nu_s, \nu_i; \nu_s-1, \nu_i+2}^N = \frac{1}{2} k'_{sii} \left[\frac{\nu_s}{2} (\nu_i+1)(\nu_i+2) \right]^{1/2}, \quad (11)$$

$$H_{\nu_s, \nu_i, \nu_j; \nu_s-1, \nu_i+1, \nu_j+1}^N = \frac{1}{2} k'_{sij} \left[\frac{\nu_s}{2} (\nu_i+1)(\nu_j+1) \right]^{1/2}, \quad (12)$$

where k'_{sab} and k'_{sfb} are chiral Fermi resonance coupling constants (see below).

In the four-dimensional case, three Darling–Dennison resonances between (ν_a, ν_b) , (ν_f, ν_b) , and (ν_f, ν_a) can be distinguished. The matrix elements of the latter are

$$H_{\nu_s, \nu_f, \nu_a; \nu_s, \nu_f-2, \nu_a+2}^N = \frac{1}{2} \delta' [\nu_f(\nu_f-1)(\nu_a+1)(\nu_a+2)]^{1/2}, \quad (13)$$

whereas the matrix elements of the Darling–Dennison resonances between ν_a and ν_b are given by

$$H_{\nu_s, \nu_a, \nu_b; \nu_s, \nu_a-2, \nu_b+2}^N = \frac{1}{2} \gamma' [\nu_a(\nu_a-1)(\nu_b+1)(\nu_b+2)]^{1/2}, \quad (14)$$

and similarly for the Darling–Dennison resonance between CF-stretching and the low frequency CD bending vibration ν_b ,

$$H_{\nu_s, \nu_f, \nu_b; \nu_s, \nu_f-2, \nu_b+2}^N = \frac{1}{2} \epsilon' [\nu_f(\nu_f-1)(\nu_b+1)(\nu_b+2)]^{1/2}. \quad (15)$$

No other quartic couplings than those responsible for the Darling–Dennison resonances had to be included. For the four-dimensional effective Hamiltonian the number of states in polyads with integral polyad quantum number N is given by Eq. (16),

$$W_{N_i}^{4D} = \frac{1}{2} \left\{ \frac{1}{3} (N+1) [4(N+1)^2 - 1] + (N+1)^2 \right\} \quad (16)$$

and with half-odd integral N it is given by Eq. (17),

$$W_{N_h}^{4D} = \frac{1}{2} (N + \frac{1}{2})(N + \frac{3}{2}) [1 + \frac{4}{3} (N+1)]. \quad (17)$$

Eigenvalues and eigenvectors of the anharmonic resonance system are obtained by diagonalization of the block-diagonal effective Hamiltonian matrix,

$$\mathbf{Z}_N^{-1} \mathbf{H}_{\text{eff}}^N \mathbf{Z}_N = \text{diag}(\Lambda_1^N, \Lambda_2^N, \dots), \quad (18)$$

where $\mathbf{H}_{\text{eff}}^N$ is one block of the full Hamiltonian matrix, \mathbf{Z}_N is the eigenvector matrix of polyad N , and $\text{diag}(\Lambda_1^N, \Lambda_2^N, \dots)$ is the diagonal eigenvalue matrix with eigenvalues Λ_i^N . The eigenstates are labeled N_j , where j increases with decreasing energy. With real $\mathbf{H}_{\text{eff}}^N$, \mathbf{Z}_N^{-1} can be replaced by the transposed matrix \mathbf{Z}_N^T .

The relative band intensities are obtained by assuming only a small number of chromophore states to carry zero order oscillator strength. The resulting relative intensities are then given by

$$g_j^N = \sum_i g_i^{(0)} |Z_{ij}^N|^2, \quad (19)$$

where the sum is extended over all zero order states with nonvanishing zero order intensity $g_i^{(0)}$. For comparison with experimental band strengths, the observed relative intensities for a polyad N are calculated by Eq. (20),

$$g_{j,\text{obs}}^N = \frac{G_{j,\text{obs}}^N}{\sum_j G_{j,\text{obs}}^N}, \quad (20)$$

where the sum is extended over all observed states of polyad N .

D. Time evolution

The time dependent wave function can be obtained for the isolated molecule, given the spectroscopic or *ab initio* Hamiltonian,⁶

$$\Psi(t) = \hat{U}(t, t_0) \cdot \Psi(t_0), \quad (21)$$

$$\hat{U}(t, t_0) = \exp[-i\hat{H} \cdot (t - t_0)/\hbar]. \quad (22)$$

In practice one uses matrix representations of the Hamiltonian (H_{mol} on a grid or H_{eff}) to compute $\Psi(t)$ or related observables derived from it. An observable we shall consider is the probability density

$$P(q_i, t) = \int \int \int |\Psi(q_i, q_j, q_k, q_l, t)|^2 dq_j dq_k dq_l, \quad (23)$$

with $\{i, j, k, l\} \in \{s, f, a, b\}$, where one can single out various coordinates q_i for observation (or graphical representation). We therefore extended our three dimensional wave packet propagation^{13,14,40} to four dimensions.

We furthermore can derive populations of basis states either for the molecular (grid) representation or the effective Hamiltonian representation.^{13,14} In the present case, we write the original grid basis (in 4D) as a direct product,

$$|q\rangle = |q_s\rangle \otimes |q_a\rangle \otimes |q_b\rangle \otimes |q_f\rangle. \quad (24)$$

This basis is then contracted by solving the one-dimensional problems for each coordinate and combining the $|q_a\rangle, |q_b\rangle, |q_f\rangle$ into a 3D basis $|\lambda_c\rangle$, giving together with one dimensional stretching functions $|\nu_s\rangle$ the four-dimensional basis with explicit stretching quantum number,

$$|\phi_{s,c}\rangle = |\nu_s, \lambda_c\rangle. \quad (25)$$

Expanding $\Psi(t)$ as

$$\Psi(t) = \sum_k b_k(t) \cdot \phi_k(q_s, q_a, q_b, q_f), \quad (26)$$

one has the population of the state k as

$$p_k^{\text{mol}}(t) = |b_k(t)|^2. \quad (27)$$

Using the effective Hamiltonian transformation for the relevant matrix representations,^{13,14}

$$\mathbf{Z}^T \cdot \mathbf{H}_{\text{eff}} \cdot \mathbf{Z} = \text{diag}(E_1, \dots, E_n), \quad (28)$$

$$\mathbf{V}^T \cdot \mathbf{H}_{\text{mol}} \cdot \mathbf{V} = \text{diag}(E_1, \dots, E_n), \quad (29)$$

$$(\mathbf{VZ}^T)^T \cdot \mathbf{H}_{\text{mol}} \cdot \mathbf{VZ}^T = \mathbf{H}_{\text{eff}}, \quad (30)$$

we can derive effective Hamiltonian basis functions as

$$\chi = \mathbf{Z} \cdot \mathbf{V}^T \cdot \phi, \quad (31)$$

with

$$\phi = (\phi_1, \phi_2, \dots, \phi_n)^T, \quad (32)$$

$$\chi = (\chi_1, \chi_2, \dots, \chi_n)^T. \quad (33)$$

Expanding $\Psi(t)$ in effective Hamiltonian basis functions one has the populations $p_k^{\text{eff}}(t)$,

$$\Psi(t) = \sum_k c_k(t) \cdot \chi_k, \quad (34)$$

$$p_k^{\text{eff}}(t) = |c_k(t)|^2. \quad (35)$$

Of course, given a matrix representation of the time evolution operator \hat{U} in any basis, one may calculate whatever observables may be of interest. For a detailed discussion of the various basis transformations, we refer to Refs. 14, 41 and for a discussion of relevant equations and practical computations of the time evolution with and without external fields we refer to Refs. 40, 42–44.

IV. SPECTROSCOPIC RESULTS

We present here a complete survey and analysis of the vibrational spectra from the lowest fundamentals in the far infrared (FIR) to the overtones in the near infrared (NIR) as far as they are relevant for the anharmonic resonance system described above. The analysis of the more detailed high resolution data will be presented elsewhere.

A. Survey of fundamentals and low energy combinations and overtones

CDBrCIF exists in four isotopomers with a natural abundance of

TABLE I. Comparison of estimated fundamentals and estimated harmonic wave numbers of the modes ν_9 to ν_1 for $\text{CD}^{79}\text{Br}^{35}\text{Cl}$ from experiment ($\bar{\nu}_i = \omega_i^{\text{exp}} + 2x_{ii} + \frac{1}{2} \sum_{j \neq i} x_{ij}$) and calculated by *ab initio* methods. The fundamentals could be assigned, due to the main contribution of internal coordinates, to local vibrations as follows: ν_9 $\angle\text{CICBr}$, ν_8 $\angle\text{FCBr}$, ν_7 $\angle\text{FCCL}$, ν_6 CBr-stretching, ν_5 CCl-stretching, ν_4 CF-stretching, ν_3 and ν_2 CD-bending and ν_1 CD-stretching.

<i>i</i>	$\bar{\nu}_i/\text{cm}^{-1}$		$\omega_i^{\text{exp}}/\text{cm}^{-1}$	ω_i/cm^{-1}		
	Obs ^a	D & B ^b	Est. ^c	MP2, Set 1	MP2, Set 2	B3LYP
9	222.7	224.2	223.5	239.36	234.29	222.81
8	312.7	313.3	317.8	326.77	326.15	311.30
7	423.2	425.0	427.4	435.10	438.88	422.48
6	619.9	620.7	627.0	641.28	654.75	616.37
5	748.37	749.7	768.5	790.17	795.62	736.32
4	1082.67	1085.0	1121.8	1108.71	1118.48	1106.93
3	917.86	919.2	937.5	1000.60	995.93	933.22
2	974.3	974.6	1004.7	1012.28	1011.57	989.29
1	2265.33	2264.0	2339.5	2391.51	2376.11	2325.80

^aObserved fundamental wave number.

^bObserved fundamentals from M. Diem and D. F. Burrow (Ref. 17).

^cObserved estimated harmonic wave number; all anharmonicities are obtained with a low order term formula Eq. (36) from experimental data (see Table VI). A full four-dimensional effective Hamiltonian analysis of the four anharmonic resonance modes ν_1 , ν_2 , ν_3 , ν_4 yields the following harmonic frequencies $\omega_i^{\text{exp,eff}}$ (in cm^{-1}): $\omega_1^{\text{exp,eff}} = 2354.3$, $\omega_2^{\text{exp,eff}} = 1006.1$, $\omega_3^{\text{exp,eff}} = 940.5$, and $\omega_4^{\text{exp,eff}} = 1119.5$.

$$\begin{array}{cccc} 0.38 & : & 0.369 & : & 0.122 & : & 0.118 \\ ^{79}\text{Br}^{35}\text{Cl} & : & ^{81}\text{Br}^{35}\text{Cl} & : & ^{79}\text{Br}^{37}\text{Cl} & : & ^{81}\text{Br}^{37}\text{Cl} \end{array}$$

The principal axes of inertia may be expected to be oriented similarly to those in CHBrCIF with the chlorine and bromine atoms lying nearly on the *a*-axis.¹² The two heavy atoms and their isotopes cause the rotational structure to be dense and congested. Because of C_1 symmetry, one finds generally hybrid bands.

The fundamentals are labeled as in CHBrCIF, i.e., with decreasing frequency, with the exception of the CF stretching mode ν_4 which has a higher frequency than the two CD bending modes ν_2 and ν_3 . Figure 1 shows an overview of the fundamental region. The fundamentals are well separated and do not overlap. Several hot band sequences with the two lowest frequency vibrations ν_9 and ν_8 are observed. The nine fundamentals are all in the region between 200 and 2300 cm^{-1} . A number of difference bands, e.g., $\nu_6 - \nu_8$, $\nu_5 - \nu_7$, etc. can also be seen. The region between 1100 and 2000 cm^{-1} shows many overlapping combination bands. All of the observed bands are assigned and are in good agreement with previous work on the fundamentals,^{17,18} to within the accuracy achievable in the early investigations.

A comparison of *ab initio* and observed harmonic wave numbers and band strengths in Tables I and II shows good agreement. As in Refs. 12, the B3LYP calculations give the best results for the harmonic wave numbers and band intensities although some harmonic wave numbers are lower than those estimated experimentally.

A comparison of isotope shifts for all five isotopomers of CDBrCIF is given in Tables III and IV. The predicted isotope shifts upon deuteration are qualitatively correct, again B3LYP calculations being most accurate, whereas for the halogenic isotopomers the predictions at the MP2 level are very good. These observations are in good agreement with Ref. 12, and our assignment of the fundamentals is consistent with *ab initio* calculations.

Table V gives a survey of all observed bands in this region. Most band centers were estimated by the maximum

TABLE II. Comparison of observed and *ab initio* band intensities for the nine fundamentals of CDBrCIF. The numbers in parentheses give the 95% confidence interval in terms of the last significant digit. No values from previous experiments are known.

Band	G/pm^2			
	$G_{\text{obs}}^{\text{exp}}$	MP2, Set 1	MP2, Set 2	B3LYP
ν_9	0.0018 ^a	0.003249	0.006462	0.004884
ν_8	0.006(1) ^a	0.01238	0.01892	0.008486
ν_7	0.029(6) ^a	0.06087	0.05380	0.0462
ν_6	0.97(5) ^a	0.8105	0.8118	1.158
ν_5	2.34(25) ^a	1.813	1.802	2.955
ν_4	2.781(55)	3.368	3.173	3.423
ν_3	2.07(11) ^{a,b}	2.223	2.479	2.635
ν_2	0.163(27)	0.6579	0.6689	0.2247
ν_1	0.0103(7) ^a	0.08907	0.08342	0.06984

^aSee Table V for notes on observed band strength.

^bPartial integration of overlapping bands.

TABLE III. Comparison of observed ($\Delta^{\text{HD}} = \tilde{\nu}_{0_i}^{\text{CH}} - \tilde{\nu}_{0_i}^{\text{CD}}$) and *ab initio* ($\Delta^{\text{HD}} = \omega_i^{\text{CH}} - \omega_i^{\text{CD}}$) isotope shifts for all nine fundamentals ν_9 to ν_1 of CD⁷⁹Br³⁵ClF vs CH⁷⁹Br³⁵ClF.

<i>i</i>	$\tilde{\nu}_{0_i}^{\text{CD}}/\text{cm}^{-1}$	$\tilde{\nu}_{0_i}^{\text{CH}}/\text{cm}^{-1}$	$\Delta^{\text{HD}}/\text{cm}^{-1}$			
			Obs.	MP2, 1	MP2, 2	B3LYP
9	222.7	223.6	0.9	1.00	1.04	0.94
8	312.7	313.0	0.3	0.67	0.74	0.68
7	423.2	425.2	2.0	2.34	2.28	2.14
6	619.9	663.6	43.7	39.13	43.67	40.38
5	748.4	787.0	38.6	48.15	50.92	34.92
4	1082.7 ^a	1077.2	-5.5	-10.85	-14.86	-7.14
3	917.9 ^a	1202.8	284.9	314.77	302.76	303.14
2	974.3 ^a	1306.2	331.9	362.95	367.01	351.82
1	2265.3	3025.5	760.2	853.50	847.75	829.99

^aThe order of modes in CDBrClF and CHBrClF is different.

of the *Q*-branch. The estimated uncertainty is of the order of 1 cm⁻¹.

The anharmonicities in Table VI have been determined either by use of the low order term formula,

$$T = \sum_i v_i \tilde{\nu}_i + \sum_j \sum_{i \leq j} x_{ij} v_i v_j, \quad (36)$$

where *T* is the transition frequency in cm⁻¹, or by use of the corresponding diagonal elements from the four dimensional effective Hamiltonian. Most of the anharmonicities are smaller than for CHBrClF as is qualitatively expected from perturbation theory.^{45,46}

B. Structure of the lower frequency fundamentals

All of the lower fundamentals show appreciable isotopic splittings. This can be seen particularly well in Fig. 4. The *Q*-branches labeled *a* are due to the ³⁷Cl isotopomers while those denoted *b* are assigned to the hot bands $\nu_8 + \nu_9 \nu_9 - \nu_9 \nu_9$ of the ³⁵Cl *Q*-branches *c*. The strongly overlapping feature near 313.8 cm⁻¹ belongs to an absorption by water. The low frequency shoulder of the partly resolved structure *b* is the barely discernible hot band due to the ³⁷Cl isotopomer. This interpretation is supported by the observed intensity ratios and high resolution spectra. Figure A.1 (Ref. 25) shows the fundamental ν_7 with comparable structure. Figure A.2 (Ref. 25) shows the fundamentals ν_6 and ν_5 at high resolution. The lower frequency fundamentals are hybrid bands with an *A*-, *B*-, and *C*-part contributing to their band contour. The band contours are very similar to CHBrClF although some bands shift considerably upon deuteration. The intensity ratio of the bands is comparable to CHBrClF where large changes of one order of magnitude between successive fundamentals are observed.¹²

C. Higher frequency fundamentals

The higher frequency fundamentals are part of the Fermi resonance system and belong therefore to the lowest two polyads, $N = \frac{1}{2}$ and $N = 1$. The states within a polyad are labeled subsequently by N_j , where $N = v_s + \frac{1}{2}v_f + \frac{1}{2}v_a + \frac{1}{2}v_b$

TABLE IV. Comparison of isotope shift for all nine fundamentals ν_9 to ν_1 for the four halogenic isotopomers of CDBrClF from experiment and as predicted from *ab initio* calculation (MP2, basis set 1). $\Delta_{\text{obs}} = \tilde{\nu}_0^{(35,79)} - \tilde{\nu}_0^{(37,79)}$ or $\Delta_{\text{obs}} = \tilde{\nu}_0^{(35,79)} - \tilde{\nu}_0^{(35,81)}$ and similarly for $\Delta_{\text{MP2},1}$. 0 has been inserted whenever the theoretical shift was smaller than 0.004 cm⁻¹ or the experimental shift could not be determined.

Band	$\Delta_{\text{obs}}/\text{cm}^{-1}$		$\Delta_{\text{MP2},1}/\text{cm}^{-1}$	
	(35,37)	(79,81)	(35,37)	(79,81)
ν_9	3.43	0.7	3.5	0.8
ν_8	0.9	0.84	0.5	0.9
ν_7	3.72	0.19	3.8	0.2
ν_6	0.8	0.9	0.5	0.5
ν_5	4.27	0	3.8	0
ν_4	0.17	0	0.03	0
ν_3	0.36	0	0.15	0.01
ν_2	0	0	0.03	0
ν_1	0	0	0	0

and *j* designates the state within the polyad. Zero order states shall be classified as $|v_s, v_f, v_a, v_b\rangle$ corresponding to ν_1 , ν_4 , ν_2 , and ν_3 .

Figure 2 shows the fundamentals ν_3 , ν_2 , and ν_4 at high resolution. The intensity pattern for these fundamentals is similar to CHBrClF. ν_4 is a near *B*-type band and the rotational structure is recognizable.

The band system between 890 and 950 cm⁻¹ shown in Fig. 2 can be assigned to the fundamental ν_3 and the combination band $\nu_6 + \nu_8$, probably strongly interacting by anharmonic coupling. Assuming no zero order intensity for the combination band, we estimate the unperturbed band centers and the coupling term

$$W_{368} = \langle v_3 = 1 | \hat{V}_{\text{anh}} | v_6 = 1, v_8 = 1 \rangle \quad (37)$$

from the perturbed band centers and the relative intensities of the two resonance components.⁴⁷ Using

$$g_{\nu_3}^{\text{per}} = \frac{G_{\nu_3}^{\text{per}}}{G_{\nu_6 + \nu_8}^{\text{per}} + G_{\nu_3}^{\text{per}}} \approx 0.8 \quad (38)$$

and perturbed band centers given in Table V, we obtain the unperturbed band centers ν_3^0 at 920.5 cm⁻¹ and $(\nu_6 + \nu_8)^0$ at 928.5 cm⁻¹ with a coupling matrix element $W_{368} = 5.3 \text{ cm}^{-1}$. Interestingly, in CHBrClF we find for the ν_3 fundamental a resonance with $\nu_5 + \nu_7$ with a coupling matrix element of 4.8 cm⁻¹.¹²

Figure 5 shows an overview of the $N=1$ polyad. We were able to assign all seven components belonging to this polyad. Component 1₂ which has mostly the character of the first overtone of the CF stretching vibration, $2\nu_4$, is approximately twice as intense as 1₁ (mostly CD stretching character, ν_1). This finding is in remarkable contrast with *ab initio* predictions (see Sec. VI), indicating that the quality of the corresponding dipole moment surface may not be sufficient to allow for an accurate calculation of band strengths in the fundamental region of CDBrClF. Similar observations were already made for CHBrClF.¹²

TABLE V. Observed wave numbers and band strengths of vibrational bands of deuterobromochlorofluoromethane. The isotopomers $\text{CD}^{79}\text{Br}^{35}\text{ClF}$, $\text{CD}^{81}\text{Br}^{35}\text{ClF}$, $\text{CD}^{79}\text{Br}^{37}\text{ClF}$, and $\text{CD}^{81}\text{Br}^{37}\text{ClF}$ are abbreviated by (79,35), (81,35), (79,37), and (81,37) respectively. The numbers in parentheses give the 95% confidence interval (where not indicated differently) in terms of the last significant digit.

	$\tilde{\nu}_0/\text{cm}^{-1}$				$G_{\text{eff}}/\text{pm}^2$	Notes
	(79,35)	(81,35)	(79,37)	(81,37)		
ν_9	222.74	221.86	219.31	218.67	0.0012	a,A,D
$\nu_6 - \nu_8$		307.1				a
ν_8	312.68	311.79	312.20	311.36	0.005(1)	a,C,D
$\nu_5 - \nu_7$		324.84		324.50		a
$\nu_6 - \nu_9$		397.07				a
ν_7	423.19	423.00	419.46	419.27	0.025(5)	a,C
$\nu_3 - \nu_7$	495.13	494.93	498.34	498.20		a,d
$\nu_8 + \nu_9$	535.66	534.01	531.80	530.16	0.0038	a
$\nu_2 - \nu_7$		549.82				a,A
$\nu_3 - \nu_8$	604.17	605.50	604.67	605.96	0.92(5)	a
ν_6	619.91	618.97	618.97	618.15		a,d,C
$2\nu_8$		625.74				b
$\nu_7 + \nu_8$	734.24	733.31	730.02	729.09	2.28(25)	a
ν_5		748.37		744.1		b
$\nu_2 - \nu_9$		749.2				a
$\nu_4 - \nu_8$		769.9				a
$\left\{ \begin{array}{l} 2\nu_7 \\ \nu_6 + \nu_9 \end{array} \right\}$		844			0.01857(67)	c
ν_3		917.86		917.50	2.49(10)	a
$\nu_6 + \nu_8$	931.21	929.50	930.28	928.49		
ν_2		974.3			0.161(27)	b
ν_4		1080.67		1082.50	2.766(55)	a
$\nu_5 + \nu_7$		1170.35		1162.87	0.0111(7)	a
$\left\{ \begin{array}{l} 2\nu_6 \\ \nu_3 + \nu_6 \end{array} \right\}$		1240			0.01811(3)	c
$\left\{ \begin{array}{l} \nu_2 + \nu_8 \\ \nu_1 - \nu_2 \end{array} \right\}$		1285.8				c,B
$\nu_3 + \nu_7$	1340.13	1339.54	1335.95	1335.27		a
$\nu_1 - \nu_3$		1347.85			0.0054(3)	b
$\nu_5 + \nu_6$	1366.79	1366.06	1361.72	1360.0		a
$\nu_4 + \nu_8$		1391.84				a
$2\nu_5$		1491.69			0.0094(2)	b
$\nu_3 + 2\nu_8$		1540.3			≈ 0.0005	b,B
$\nu_2 + \nu_6$	1591.91	1590.9	1590.9	1589.80	0.00039(5)	b
$\nu_3 + \nu_5$		1663.33		1658.70	0.0020(1)	a
$\nu_4 + \nu_6$		1700.5				d
$2\nu_3$		1828			≈ 0.001	d,B
$\nu_4 + \nu_5$		1830.13		1825.82	≈ 0.0009	a,B
$\nu_2 + \nu_3$		1889.82		1889.36	0.0027(1)	a
$\nu_2 + \nu_6 + \nu_8$	1903.01	1901.28				a
$2\nu_2$		1941.67				a
$\nu_2 + \nu_4$		2041.95		2041.68	0.0022(2)	a
$2\nu_4$		2145.14			0.0212(8)	b
ν_1	2265.33	2265.27	2264.98		0.0103(7)	a,E
$\nu_1 + \nu_9$		2487.68			0.00008	b
$\nu_1 + \nu_8$		2578.66				b,e
$\nu_1 + \nu_7$	2688.91	2688.67	2684.78	2684.48		a
$\nu_1 + \nu_6$		2883.51			0.00033(2)	b
$\nu_1 + \nu_5$		3009.71		3005.99	0.00041(3)	a

Notes: Observed wave numbers of vibrational bands of CDBrClF.

The reported band centers $\tilde{\nu}_0$ are derived from:

^aMaximum of the Q branch, estimated uncertainty, $\pm 0.5 \text{ cm}^{-1}$.

^bMinimum between P and R branch, estimated uncertainty, $\pm 0.7 \text{ cm}^{-1}$.

^c“Center of gravity” of the band, estimated uncertainty, $\pm 1.0 \text{ cm}^{-1}$.

^dShoulder; approximate maximum of Q branch, estimated uncertainty, $\pm 1.0 \text{ cm}^{-1}$.

^(A)Band strength obtained from one measurement only.

^(B)Very weak transition; the band strength can only be estimated roughly.

^(C)Band strength obtained from two measurements only.

^(D) H_2O lines overlap and contribute to band strength.

^(E) $^{13}\text{CO}_2$ lines overlap; the band strength contains some contributions of the $(0,0^0,1)-(0,0^0,0)$ transition.

TABLE VI. Anharmonicity constants of CDBrClF. It is assumed that the anharmonicities are to a good approximation identical for all four isotopomers.

<i>i</i>	<i>j</i>	x_{ij}/cm^{-1}	Source	<i>i</i>	<i>j</i>	x_{ij}/cm^{-1}	Source
1	1	-27.5 ^a	$2\nu_1$	2	6	-2.2	$\nu_2 + \nu_6$
2	2	-2.0 ^a	$2\nu_2$	3	4	-0.7 ^a	$\nu_3 + \nu_4$
3	3	-5.1 ^a	$3\nu_3$	3	5	-3.4	$\nu_3 + \nu_5$
4	4	-10.2 ^a	$2\nu_4$	3	7	-1.3	$\nu_3 + \nu_7$
5	5	-5.1	$2\nu_5$	3	9	-0.4	$\nu_3 + \nu_9 - \nu_9$
1	2	-9.8 ^a	$\nu_1 + \nu_2$	4	5	-0.6	$\nu_4 + \nu_5$
1	3	-2.7 ^a	$\nu_1 + \nu_3$	4	8	-3.9	$\nu_4 + \nu_8$
1	4	^a		5	6	-1.1	$\nu_5 + \nu_6$
1	5	-3.5	$\nu_1 + \nu_5$	5	7	-0.6	$\nu_5 + \nu_7$
1	6	-2.4	$\nu_1 + \nu_6$	5	9	-0.7	$\nu_5 + \nu_9 - \nu_9$
1	7	-0.2	$\nu_1 + \nu_7$	6	8	-1.4	$\nu_6 + \nu_8$
1	8	0.3	$\nu_1 + \nu_8$	7	8	-1.7	$\nu_7 + \nu_8, \nu_8 + \nu_7 - \nu_8$
1	9	-0.9	$\nu_1 + \nu_9, \nu_9 + \nu_1 - \nu_9$	7	9	-0.4	$\nu_7 + \nu_9 - \nu_9$
2	3	-0.9 ^a	$\nu_2 + \nu_3$	8	9	-1.6	$\nu_8 + \nu_9$
2	4	-13.5 ^a	$\nu_2 + \nu_4$				

^aAnharmonicity constants as estimated by the four dimensional effective Hamiltonian are: $x'_{11} = -34.99(79) \text{ cm}^{-1}$, $x'_{22} = -1.59(54) \text{ cm}^{-1}$, $x'_{33} = -4.6(13) \text{ cm}^{-1}$, $x'_{44} = -10.01(21) \text{ cm}^{-1}$, $x'_{12} = -12.7(17) \text{ cm}^{-1}$, $x'_{13} = -5.9(32) \text{ cm}^{-1}$, $x'_{14} = 2.56(89) \text{ cm}^{-1}$, $x'_{23} = -1.9(15) \text{ cm}^{-1}$, $x'_{24} = -12.5(11) \text{ cm}^{-1}$, $x'_{34} = -1.97(80) \text{ cm}^{-1}$, where the numbers in parentheses give the estimated standard deviation in terms of the last significant digit.

V. OVERTONE SPECTRA AND ANHARMONIC RESONANCE ANALYSIS

A. Survey of overtone spectra

Figure 6 shows an overview of the resonance structure in the region covered. Table VII gives a complete listing of all observed bands, with assignments according to the four-dimensional effective Hamiltonian with $N = \nu_s + \frac{1}{2}\nu_f + \frac{1}{2}\nu_a + \frac{1}{2}\nu_b$.

The spectra of the overtone region of CDBrClF are dominated by combination and overtone bands of the highest four fundamentals. These build a complex band system caused by Fermi and Darling–Dennison resonances. Different from CHBrClF, the CF-stretching mode ν_4 is now part of the polyads because of the near resonance of ν_1 and $2\nu_4$. The anharmonicity of the CD stretching vibration is smaller than for the corresponding CH stretching mode in CHBrClF, and the whole spectral pattern is shifted to lower wave num-

bers upon deuteration. The same tendency of band strength fall-off is found for both integral and half-integral polyads, i.e., about one order of magnitude per polyad. Absorption from CHBrClF impurities become dominant in the higher polyads because of the higher excitation of the CD-modes compared to the CH-modes at the same wavenumber. We used this effect to estimate the isotopic purity of our sample, because the absolute band strengths for CHBrClF are known.¹²

Figure 7 shows polyads $N=2$ and $N=3$. The bands exhibit the typical contour also observed in CHBrClF. In polyad $N=3$, the intensity maximum appears at the component 3_2 . Because of the anharmonic resonances, $3\nu_1$ (attrib-

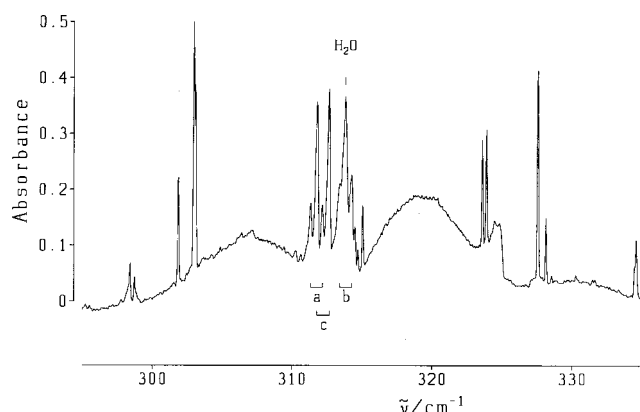


FIG. 4. The fundamental ν_8 . Q-branches (a) ^{37}Cl isotopomer; (b) $\nu_8 + \nu_9\nu_9 - \nu_9\nu_9$ hot band due to ^{35}Cl isotopomer; (c) ^{35}Cl isotopomer. The strongly interfering lines are due to absorption of water. Conditions: room temperature, resolution 0.1 cm^{-1} , $l = 14 \text{ m}$, $p = 6.31 \text{ mbar}$.

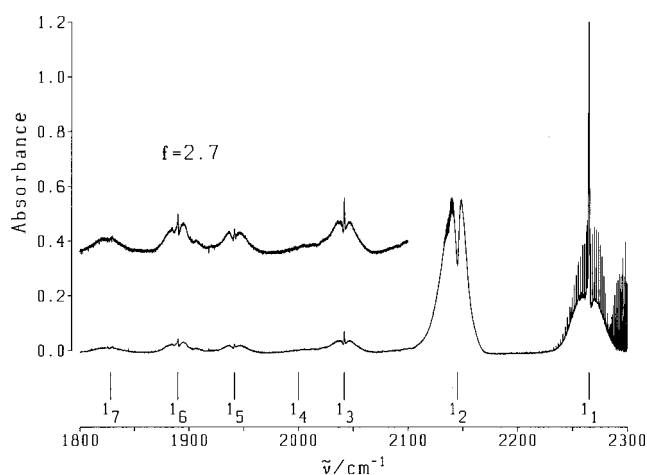


FIG. 5. Spectrum of polyad $N=1$ in terms of the reduced absorbance $f \cdot \ln(I_0/I)$. All seven components belonging to this polyad are observed. The ticks give the assignment of these bands according to the four-dimensional effective Hamiltonian. Traces of CO_2 are seen at $\approx 2280 \text{ cm}^{-1}$ and of $^{13}\text{CO}_2$ at lower wave numbers, overlapping with 1_1 . Conditions: room temperature, resolution 0.1 cm^{-1} , $l = 18 \text{ cm}$. Lower trace: $p = 72.71 \text{ mbar}$, $f = 1$; upper trace: $p = 198 \text{ mbar}$, $f = 2.7$.

TABLE VII. Complete listing of all observed bands in the overtone region of CDBrClF. Where it is not noted otherwise, the transition wave number is determined at the maximum of the Q -branch. The numbers in parentheses give the 95% interval in terms of the last significant digit.

	$\tilde{\nu}_0/\text{cm}^{-1}$	$G_{\text{eff}}/\text{km}^{-2}$	Notes		$\tilde{\nu}_0/\text{cm}^{-1}$	$G_{\text{eff}}/\text{km}^{-2}$	Notes
$(\frac{1}{2})_3$	917.9	2.04(1)	A	$(\frac{5}{2})_1$	5575.8	$2.0 \cdot 10^{-6}$	C
$(\frac{1}{2})_2$	972.8	0.161(3)		$(2_1)^{\text{CH}}$	5928.1	$1.42(5) \cdot 10^{-5}$	E
$(\frac{1}{2})_1$	1082.7	2.77(6)		3_{17}	6113.3	$1.1 \cdot 10^{-7}$	C
1_7	1828.0	0.00097		3_{13}	6226.6	$8.4 \cdot 10^{-7}$	C
1_6	1889.8	0.00126(1)		3_{10}	6289.5	$1.9 \cdot 10^{-6}$	C
1_5	1941.7	0.0011(1)		3_8	6371.5	$\} 1.0 \cdot 10^{-6}$	C,G
1_4	1999.9	$\} 0.0022(2)$		3_6	6384.5		C,G
1_3	2042.0			3_4	6488.0	$\} 7.2 \cdot 10^{-6}$	C
1_2	2145.2	0.0212(8)		3_3	6501.9		C
1_1	2265.3	0.0103(7)	B	3_2	6579.8	0.000015	C
$\nu_1 + \nu_9$	2487.7	0.000017(1)	a,C	3_1	6672.6	$3.4 \cdot 10^{-6}$	C
$\nu_1 + \nu_7$	2688.9	0.000012(1)	C	$(\frac{5}{2})_2^{\text{CH}}$	7103.0	$6.1(2) \cdot 10^{-7}$	E
$(\frac{3}{2})_{13}$	2723.0	0.000019(8)		$(\frac{5}{2})_1^{\text{CH}}$	7201.9	$3.55(2) \cdot 10^{-7}$	E
$(\frac{3}{2})_{12}$	2795.0	$\approx 5 \cdot 10^{-6}$	D	$(\frac{7}{2})_{13}$	7320.0	$4.6 \cdot 10^{-7}$	C,G
$\nu_1 + \nu_6$	2883.5	0.00036(2)	a,C	$(\frac{7}{2})_9$	7415.0	$\} 2.6 \cdot 10^{-7}$	C,G
$\nu_1 + \nu_5$	3009.7	0.00040(5)	C	$(\frac{7}{2})_8$	7434.0		C,G
ν_1^{CH}	3025.5	$7(3) \cdot 10^{-6}$	E	$(\frac{7}{2})_6$	7491.4	$\} 3.6 \cdot 10^{-7}$	C,G
$(\frac{3}{2})_6$	3061.3	0.000044(7)		$(\frac{7}{2})_5$	7516.0		C,G
$(\frac{3}{2})_5$	3090.6	0.000050(27)		$(\frac{7}{2})_3$	7580.5	$1.7 \cdot 10^{-7}$	C,G
$(\frac{3}{2})_4$	3180.5	$\} 0.00095(7)$		$(3_4)^{\text{CH}}$	8252.5	$3 \cdot 10^{-8}$	E
$(\frac{3}{2})_3$	3188.3			4_{14}	8390.1		F
$(\frac{3}{2})_2$	3228.3	0.00048(4)		$(3_2)^{\text{CH}}$	8453.0	$7 \cdot 10^{-8}$	E
$(\frac{3}{2})_1$	3356.5	0.00039(3)		4_7	8550.9	$\approx 1 \cdot 10^{-7}$	D,G
2_{10}	4083.8	0.0003(1)		4_5	8631.6	$\approx 4 \cdot 10^{-7}$	D
2_6	4188.1		F	$(3_1)^{\text{CH}}$	8711.5	$5.1(5) \cdot 10^{-7}$	E
$(\frac{3}{2})_2^{\text{CH}}$	4210.0	$3(1) \cdot 10^{-5}$	a,A,E	CHCl_3	8725.6		E
2_3	4302.2	0.00034(10)		4_1	8850.9		F
2_2	4408.4	0.00037(10)		$(\frac{9}{2})_{23}$	9361	$\approx 1 \cdot 10^{-8}$	D,G
2_1	4475.7	0.0011(1)		$(\frac{9}{2})_{17}$	9430	$\approx 1 \cdot 10^{-8}$	D,G
$2\nu_1 + \nu_9$	4698.9	$\approx 5 \cdot 10^{-7}$	a,D	$(\frac{9}{2})_{12}$	9540	$\approx 8 \cdot 10^{-9}$	D,G
$2\nu_1 + \nu_7$	4897.4	$\approx 5 \cdot 10^{-7}$	a,D	$(\frac{9}{2})_6$	9625	$\approx 4 \cdot 10^{-9}$	b,D,G
$(\frac{5}{2})_{19}$	4976.4	$1.7 \cdot 10^{-6}$	C	$(\frac{7}{2})_3^{\text{CH}}$	9684.7		E,F
$(\frac{5}{2})_{17}$	5027.0	$2.4 \cdot 10^{-6}$	A,C	$(\frac{7}{2})_2^{\text{CH}}$	9873.0	$1 \cdot 10^{-8}$	E
$(\frac{5}{2})_{15}$	5044.1	$2.3 \cdot 10^{-6}$	A,C	CHCl_3	9899.0		E
$2\nu_1 + \nu_6$	5090.1	$\approx 4 \cdot 10^{-6}$	D	$(\frac{7}{2})_1^{\text{CH}}$	9973.1		E,F
$(\frac{5}{2})_{11}$	5144.7	$4.9 \cdot 10^{-6}$	A,C	5_{23}	10440	$\approx 1 \cdot 10^{-9}$	D,G
$\nu_1 + 2\nu_4 + \nu_5$	5157.2	$\approx 3 \cdot 10^{-6}$	a,D	5_{13}	10557	$\approx 3 \cdot 10^{-9}$	D,G
$2\nu_1 + \nu_5$	5219.0	$\approx 9 \cdot 10^{-6}$	a,D	5_9	10638	$\approx 8 \cdot 10^{-9}$	D,G
$(\frac{5}{2})_7$	5245.0	$\approx 3 \cdot 10^{-6}$	D	5_5	10730	$\approx 1 \cdot 10^{-9}$	D,G
$(\frac{5}{2})_6$	5327.1	$\} \approx 0.00001$	D	$(4_2)^{\text{CH}}$	11201.9		E,F
$(\frac{5}{2})_5$	5348.5		D	$(4_1)^{\text{CH}}$	11376.2	$1.7 \cdot 10^{-8}$	E
$(\frac{5}{2})_4$	5385.8	$\} 0.000037$	C				
$(\frac{5}{2})_3$	5424.0		C				

^aThe reported band centers $\tilde{\nu}_0$ are determined at the minimum of the Q branch.

^bAssignment not conclusive.

^(A)Partial integration of overlapping bands.

^(B) $^{13}\text{CO}_2$ lines overlap; the band strength contains some contributions of the $(0,0^0,1)-(0,0^0,0)$ transition.

^(C)Band strength obtained from two measurements only.

^(D)Band strength obtained from one measurement only; indicates order of magnitude only.

^(E) $x_{\text{CH}} G_{\text{eff}}$ instead of G_{eff} , where $x_{\text{CH}}=0.37(11)\%$ is the mole fraction of CHBrClF in the sample.

^(F)Very weak transition; the band strength cannot be determined.

^(G)Broad band possibly overlapping with other bands; indicates order of magnitude only.

uted approximately to 3_2) is about 10 cm^{-1} lower than predicted on the basis of the spectroscopic constants of polyad $N=1$ and the term formula to low order, Eq. (36). Some bands overlap strongly. One observes some bands belonging

to polyads $N=\frac{3}{2}$ and $N=2$ of CHBrClF, being strong despite the low partial pressure of CHBrClF in the sample (mole fraction of CHBrClF in CDBrClF $x_{\text{CH}}=0.0037 \pm 0.0011$).

Figure 8 shows the survey spectrum of polyad $N=\frac{3}{2}$.

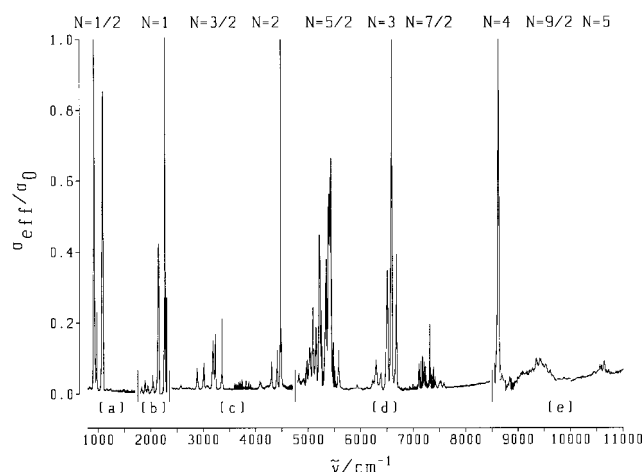


FIG. 6. Survey of all polyads from $N = \frac{1}{2}$ to $N = 5$. The spectrum is given in terms of a relative observed absorption cross section $\sigma_{\text{eff}}/\sigma_0$ at a resolution of 0.1 cm^{-1} , where the conditions for parts (a)–(e) are (a) $l = 18 \text{ cm}$, $p = 3.05 \text{ mbar}$, $\sigma_0 = 158.88 \text{ pm}^2$; (b) $l = 18 \text{ cm}$, $p = 72.71 \text{ mbar}$, $\sigma_0 = 4.37 \text{ pm}^2$; (c) $l = 18 \text{ cm}$, $p = 477.6 \text{ mbar}$, $\sigma_0 = 0.89 \text{ pm}^2$; (d) $l = 4200 \text{ cm}$, $p = 305 \text{ mbar}$, $\sigma_0 = 4.11 \cdot 10^{-3} \text{ pm}^2$; (e) $l = 6000 \text{ cm}$, $p = 273.5 \text{ mbar}$, $\sigma_0 = 1.75 \cdot 10^{-4} \text{ pm}^2$. The regions near 3200 cm^{-1} , 5300 cm^{-1} , and 7200 cm^{-1} are blurred by absorptions due to water. The strong absorptions due to CHBrClF in the region of 8700 cm^{-1} and 9800 cm^{-1} are reduced by a factor of 100 and 10, respectively.

The polyad components 12 and 13, which carry mostly bending overtone character and those components with predominant ν_a and ν_b character are weak, the strongest bands involving the CF stretching vibration. This is seen throughout the spectrum. The zero order state $|1, 1, 0, 0\rangle$ is shifted towards higher wave numbers with respect to predictions based on the low order term formula, indicating again the importance of off-diagonal anharmonic terms. Figures of the remaining polyads are shown in EPAPS.²⁵ For $N = \frac{5}{2}$ many bands provide a dense, partly overlapping spectrum. The assignment of band centers is corroborated by predictions based on the effective Hamiltonian. Combination bands of ν_1 and the strong lower fundamentals, $2\nu_1 + \nu_i$, $i \in \{5, 6, 7, 9\}$, fall into the region of this polyad. The strong Q -branch in the highest band of the polyad is due to CHBrClF . In polyad $N = \frac{7}{2}$ the intensity is distributed evenly among the higher states of the polyad, the absorbance being generally weak. The band at approximately 7202 cm^{-1} is the highest state in $N = \frac{5}{2}$ of CHBrClF . Polyad $N = 4$ shows the typical structure as observed in the lower integral polyads. The bands are quite broad with small or no distinct Q -branches. 4_2 is covered by the much stronger 3_1 band of CHBrClF . Based on the effective Hamiltonian analysis, a rough estimate of the band position is given by $\tilde{\nu}_0(4_2) \approx 8710 \pm 10 \text{ cm}^{-1}$. This band might be detectable by isotope selective overtone spectroscopy (ISOS).⁴⁸ Two more states belonging to $N = 3$ of CHBrClF are also observed. The two polyads $N = \frac{9}{2}$ and $N = 5$ are dominated by broad, weak and overlapping spectral features. The peak positions are roughly estimated and an assignment is proposed by the effective Hamiltonian. The complete set of spectra is reproduced in the figures of EPAPS.²⁵

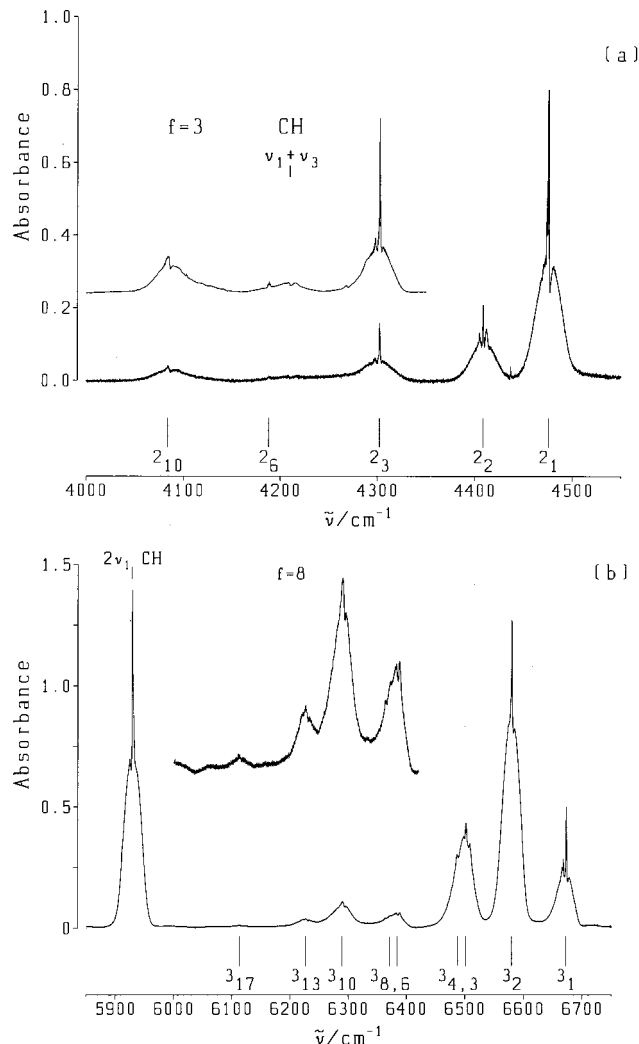


FIG. 7. (a) and (b) Survey spectra of polyads $N = 2$ and $N = 3$ in terms of reduced absorbance $f \cdot \ln(I_0/I)$. The ticks give the assignment of the bands according to the four-dimensional effective Hamiltonian. Conditions: room temperature, resolution 0.1 cm^{-1} . (a) $N = 2$. The band at 4210 cm^{-1} belongs to the CH chromophore in CHBrClF . Upper trace: $l = 2100 \text{ cm}$, $p = 57.75 \text{ mbar}$, $f = 3$; lower trace: $l = 18 \text{ cm}$, $p = 477.6 \text{ mbar}$, $f = 1$. (b) $N = 3$. The band at 5928 cm^{-1} is $2\nu_1$ of CHBrClF , $l = 4200 \text{ cm}$, $p = 305 \text{ mbar}$. Upper trace: $f = 8$. Lower trace, $f = 1$.

B. Effective Hamiltonian analysis

Table VIII gives the results for effective Hamiltonian parameters as obtained from experimental data and, for comparison, obtained from a fit to *ab initio* data. Where parameters were not well determined in the fit procedure, they have been determined by a best fit to experimental intensities, using $g_{\text{eff}}^{(0)}(|N, 1, 0\rangle) = 0.01$, $g_{\text{eff}}^{(0)}(|N, 0, 1\rangle) = 0.2$, $g_{\text{eff}}^{(0)}(|N - 1, 3, 0\rangle) = 0.01$ and $g_{\text{eff}}^{(0)}(|N, 0, 0\rangle) = 0.7$, $g_{\text{eff}}^{(0)}(|N - 1, 1, 1\rangle) = 0.2$ in $\hat{H}_{\text{eff}}^{3D,F}$ and $g_{\text{eff}}^{(0)}(|N, 0, 0, 0\rangle) = 1.0$, $g_{\text{eff}}^{(0)}(|N - 1, 0, 1, 1\rangle) = 0.0$, $g_{\text{eff}}^{(0)}(|N, 1, 0, 0\rangle) = 0.03$, $g_{\text{eff}}^{(0)}(|N, 0, 0, 1\rangle) = 0.01$, and $g_{\text{eff}}^{(0)}(|N, 0, 1, 0\rangle) = 0.2$ for $\hat{H}_{\text{eff}}^{4D}$. The zero order intensity assumptions are justified by the observation that in all polyads at least two or three transitions are nearly equally intense; the magnitude of the zero order intensities are chosen so as to represent the experimental intensities best. We emphasize that the parameters demonstrate conclusively the importance of the CF stretching vibration in the Fermi reso-

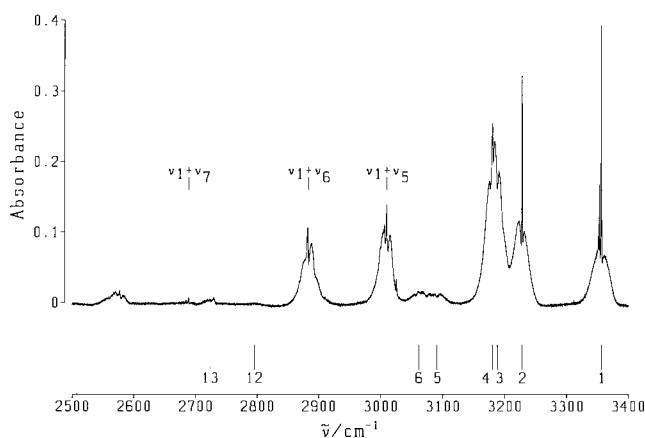


FIG. 8. Survey spectrum of polyad $N=3/2$. Also observed are combination bands with strong low fundamentals, $\nu_1 + \nu_5$, $\nu_1 + \nu_6$ and $\nu_1 + \nu_7$. The ticks indicate the assignment according to the four-dimensional effective Hamiltonian. Conditions: room temperature, resolution 0.1 cm^{-1} , $l=18 \text{ cm}$, $p=477.6 \text{ mbar}$.

nance system of CDBrClF, quite in contrast to CHBrClF. The comparison of parameters obtained by $\hat{H}_{\text{eff}}^{4D}$ and $\hat{H}_{\text{eff}}^{3D,F}$ shows excellent agreement between the two sets of data. However, the parameters describing the coupling with ν_b are not well determined due to the small number of observed bands involving ν_b . The parameters γ' and δ' are small and not well determined experimentally. In Table VIII we have considered only one of the several possible sign combinations for the coupling constants best fitting the *ab initio* data. For a detailed discussion see Ref. 12.

VI. ANHARMONIC RESONANCE ANALYSIS USING 3D AND 4D POTENTIAL ENERGY AND DIPOLE MOMENT FUNCTIONS

As a second step towards an understanding of the anharmonic resonances in CDBrClF, we calculated the potential energy and the dipole moment surfaces as described above. A few representative cuts through the potential energy surface are shown in Fig. 9. The potential energy cuts along q_s, q_f , along q_s, q_a and along q_s, q_b all show the typical kidneylike structure characteristic of strong Fermi resonances. The sections in q_s with q_f and q_s with q_a as well as q_s with q_b have a rather similar shape, indicating a similarly strong Fermi resonance coupling. The dipole moment surface cuts, shown in EPAPS (Ref. 25) as the components along the principal inertial axes a, b, c , demonstrate the significant differences from the usual assumption of linear and other simple one-dimensional dipole moment functions.

On the basis of the four-dimensional potential energy and dipole moment surfaces, we calculated vibrational band centers and absolute intensities up to high overtones. The predicted transition frequencies from the *ab initio* calculations, MP2 (basis set 1), compared to the experimentally observed frequencies are systematically too high by about 10%. This is inadequate, particularly for the prediction of yet unobserved band centers. We therefore adjusted the potential energy surface in normal coordinate space by scaling the harmonic wave numbers, as defined by Eq. (39),

TABLE VIII. Comparison of effective parameters as obtained from the different effective hamiltonians on experimental and experimentally scaled MP2 *ab initio* spectra. Fitting without adjusting those parameters that are not well determined (standard deviation larger than absolute value of parameter) yields for the experimental parameters: $k_{saa}^{3D,F}=15(17) \text{ cm}^{-1}$, $\gamma^{3D,F}=1(2) \text{ cm}^{-1}$, while all other parameters change only little if at all. For the four-dimensional effective Hamiltonian on the *ab initio* data only data up to $N=4$ and a small number belonging to $N=9/2$ and $N=5$ are included. The numbers in parentheses give the standard deviation in terms of the last significant digits.

Parameter/ cm^{-1}	$\hat{H}_{\text{eff}}^{3D,F}$	$\hat{H}_{\text{eff}}^{4D}$	$\hat{H}_{\text{eff,MP2}}^{3D,F}$	$\hat{H}_{\text{eff,MP2}}^{4D}$
$\tilde{\nu}'_s$	2293.8(17)	2291.2(19)	2296.0(10)	2285.8(15)
$\tilde{\nu}'_f$	1092.6(12)	1094.4(10)	1084.62(44)	1088.22(68)
$\tilde{\nu}'_a$	974.1(19)	974.9(16)	971.70(46)	974.22(71)
$\tilde{\nu}'_b$...	923.1(24)	...	919.2(7)
x'_{ss}	-34.98(49)	-34.99(79)	-32.12(29)	-34.30(56)
x'_{ff}	-9.61(28)	-10.01(21)	-5.725(73)	-6.99(12)
x'_{aa}	-0.54(63)	-1.59(54)	-1.20(16)	-1.91(18)
x'_{bb}	...	-4.6(13)	...	-1.24(27)
x'_{sf}	4.3(76)	2.56(89)	-0.78(23)	-5.59(51)
x'_{sa}	-14.8(73)	-12.7(17)	-15.0(54)	-17.33(74)
x'_{sb}	...	-5.9(32)	...	-17.24(83)
x'_{fa}	-12.1(74)	-12.5(11)	-7.21(21)	-5.16(37)
x'_{fb}	...	-1.97(80)	...	0.18(40)
x'_{ab}	...	-1.9(15)	...	1.40(41)
k'_{sff}	38.2(13)	41.2(14)	50.41(62)	50.7(11)
k'_{saa}	30.6	24(20)	54.3(29)	39.5(34)
k'_{sbb}	...	57(23)	...	59.8(44)
k'_{sfa}	68.6(32)	67.7(56)	71.5(17)	98.0(32)
k'_{sfb}	...	-19(13)	...	-91.3(36)
k'_{sab}	...	0(40)	...	91.8(45)
γ'	...	2(15)	...	-1.1(8)
δ'	2.9	...	1.84(64)	-1.7(7)
ϵ'	4.0(12)
d_{rms}	3.12	2.43	2.76	3.65
n_{data}	43	58	160	301

$$\omega_i^{\text{scal}} = \left(\frac{\omega_i^{\text{obs}}}{\omega_i^{\text{MP2}}} \right)^2 \omega_i^{\text{MP2}} \approx \left(\frac{\tilde{\nu}_{0i}^{\text{obs}}}{\tilde{\nu}_{0i}^{\text{MP2}}} \right)^2 \omega_i^{\text{MP2}}; \quad i \in \{s, f, a, b\}, \quad (39)$$

where ω_i^{scal} , ω_i^{obs} , ω_i^{MP2} , $\tilde{\nu}_{0i}^{\text{obs}}$, and $\tilde{\nu}_{0i}^{\text{MP2}}$ are the scaled harmonic, the observed harmonic, the *ab initio* harmonic, the observed fundamental transition and the *ab initio* fundamental transition wave numbers of the normal mode i . In practice we have used the second part in Eq. (39). Such a scaling procedure leads to acceptable predictions of the overtone spectra on the basis of the adjusted potential although more refined adjustments are possible.^{12,13,35}

Figure 10 shows in its upper part a survey of the calculated absorption patterns, agreeing quite well with the experimental patterns in Fig. 6. Table VIII shows a comparison of the effective parameters as obtained from the different models by fitting observed or calculated band positions to a 3D and 4D model effective Hamiltonian \hat{H}_{eff} . Effective parameters in the fit to three and four dimensional *ab initio* data are consistent, as already observed for the fit to experimental data. Moreover, *ab initio* and experimental *effective parameters* agree very well, although the corresponding *spectra* show too large relative shifts to allow for a direct quantitative comparison (cf. also Ref. 12). One finds also correla-

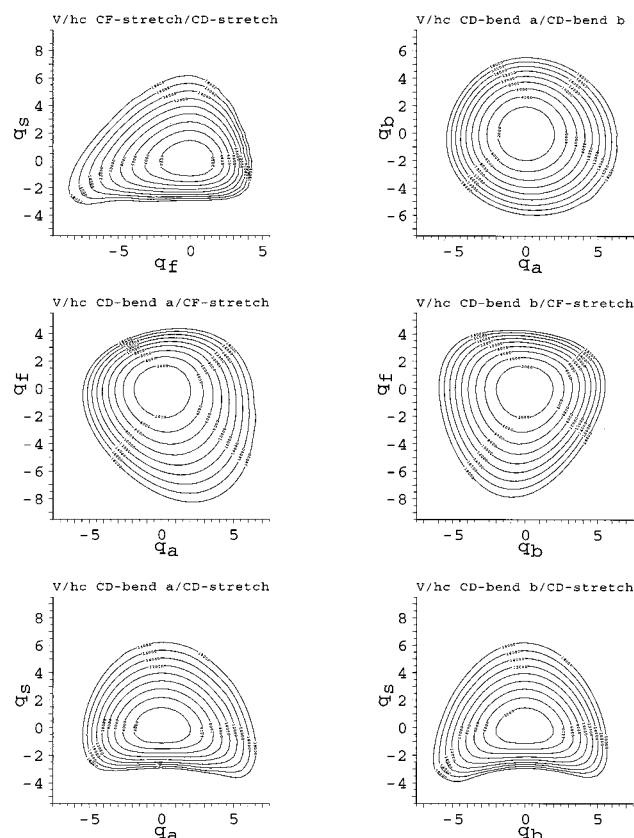


FIG. 9. Representative two dimensional cuts near the minimum of the pure *ab initio* potential energy surface of the four-dimensional Fermi resonance subspace in reduced rectilinear normal coordinates q_s , q_f , q_a , and q_b (MP2, basis set 1). In each diagram the innermost contour is at 2000 cm^{-1} , the following contours increasing in steps of 2000 cm^{-1} up to a maximum of $18\,000\text{ cm}^{-1}$. Negative values of the reduced coordinate q_f correspond to positive extensions of the CF bond from its equilibrium value.

tions of pairs of parameters which may lead to slightly different analyses of *ab initio* and experimental spectra in terms of effective parameters. Also, the assignment of *ab initio* bands to the higher polyads $N > 4$ in the four-dimensional effective Hamiltonian is particularly difficult due to the large density of states. For this model we present therefore an analysis of *ab initio* data up to polyad $N = 4$. Since the Fermi resonance structure is dominated by the modes ν_s and ν_f , the anharmonic parameters involving these modes are well determined, better than the effective parameters k'_{saa} , k'_{sab} , and k'_{sbb} . Differences of these effective parameters in the three and four-dimensional models may arise because they are mainly determined by band centers in the higher polyads and thus remain relatively uncertain. Effective fit parameters which are not well determined (standard deviation of the same order of magnitude as the parameter) have been fixed to a value so as to reproduce either the relative intensities of the *ab initio* or of the experimental data.

Including all variationally calculated bands in the fit, instead of only those corresponding to observed transitions, does not change the parameters significantly; this is an indication that the anharmonic resonance system is described adequately by the *observed* bands and hence by the effective Hamiltonian. This is also supported by the very small root-mean-square deviation of the fit ($d_{\text{rms}} \approx 3.7\text{ cm}^{-1}$) for 301

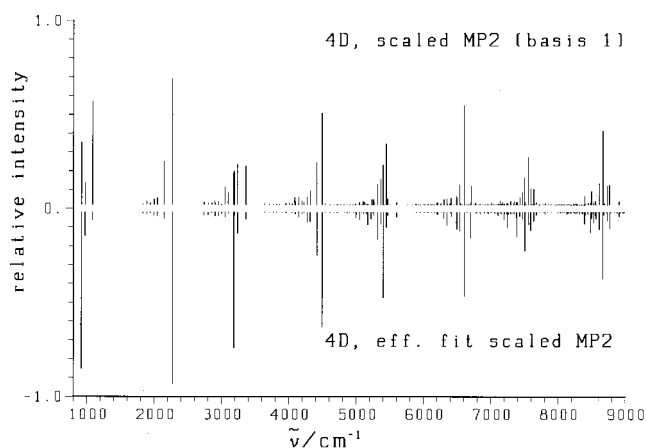


FIG. 10. Survey of band positions and relative intensities as calculated with $\hat{H}_{\text{eff}}^{4D}$ and with potential energy and dipole moment surfaces from scaled *ab initio* data (MP2, basis set 1). Data up to $N = 4$ are shown. The scaling factors for absolute intensities G in the upper part of the figure are in order of the polyads: 6.09 pm^2 , 0.14 pm^2 , 0.0029 pm^2 , $0.001\,02\text{ pm}^2$, 40.91 fm^2 , 41.67 fm^2 , 0.874 fm^2 , 1.49 fm^2 . The lower mirror image part shows the corresponding *relative* intensities within each polyad from the effective Hamiltonian adjusted to the scaled *ab initio* data.

fitted band centers. A complete list of the calculated band centers and intensities can be found in EPAPS (Table A.5).²⁵ The importance of the symmetry-breaking parameters k'_{sfb} and k'_{sab} has been checked in $\hat{H}_{\text{eff},\text{MP2}}^{4D}$ by setting them to zero (see below), which resulted in a somewhat less satisfactory numerical fit with $k'_{sfa} = 49.5(44)\text{ cm}^{-1}$, i.e., smaller than k'_{sff} ($54.5(10)\text{ cm}^{-1}$), in disagreement with the results from *all* other models. The parameter k'_{saa} remains then undetermined. It is therefore necessary to include the two chiral effective Fermi resonance coupling constants k'_{sfb} and k'_{sab} to successfully model the overtone spectrum of this four dimensional anharmonic resonance system.

Figure 10 also compares the scaled (MP2) *ab initio* spectra for $N \leq 4$ with those obtained from $\hat{H}_{\text{eff}}^{4D}$ as fitted to the scaled *ab initio* spectrum. The relative intensities in each polyad are shown as mirror images in the lower part of the figure. The intensities in the polyads with integer N from $N = 2$ to $N = 4$ are described well by the effective Hamiltonian with a tendency of slightly overestimating the relative intensities of the polyad's highest bands. In the lower polyads $N = \frac{1}{2}$ and $N = \frac{3}{2}$ one finds large differences between the accurately calculated intensities and the effective Hamiltonian model. This discrepancy is expected because here the intensities are largely determined by the electric dipole function and not the anharmonic resonance coupling to some chromophore states. Furthermore, the half-odd integer N polyads show considerably more overlapping band centers of similar intensity than integral polyads, which renders the experimental determination of intensities difficult. This must be considered when comparing theoretical with experimental intensities.

While the scaled *ab initio* and experimental relative intensities in the higher polyads are in good agreement, this is not true for the absolute and relative intensities of the fundamentals and low overtones. Striking examples are provided by the relative and absolute intensities of ν_s and ν_a , as well

TABLE IX. Parameters $C_{s^i f j a^k b^l}$ of the Taylor series expansion of the MP2 (basis set 1) *ab initio* potential for an adjustment to: Fourth order and a limiting potential energy of 6000 cm^{-1} , columns I and III; fifth order and a limiting potential energy of 15 000 cm^{-1} , columns II and IV.

<i>i</i>	<i>j</i>	<i>k</i>	<i>l</i>	$C_{s^i f j a^k b^l} / \text{cm}^{-1}$			
				MP2		MP2 scaled	
				I	II	III	IV
2	0	0	0 ^a	1195.75	1195.75	1130.36	1130.36
0	2	0	0 ^a	554.35	554.35	549.40	549.40
0	0	2	0 ^a	506.14	506.14	480.66	480.66
0	0	0	2 ^a	500.30	500.30	431.71	431.71
0	2	1	0	-53.02(75)	-53.67(57)	-53.8(15)	-54.18(81)
0	3	0	0	65.20(50)	65.51(31)	66.66(98)	66.03(41)
1	0	2	0	69.7(11)	91.1(11)	82.7(21)	79.3(17)
1	0	1	1	58.7(13)	74.8(15)	62.2(24)	67.2(24)
1	1	1	0	92.4(15)	126.0(16)	94.9(30)	116.3(24)
1	0	0	2	107.7(10)	139.2(10)	127.6(20)	113.4(16)
1	1	0	1	-48.2(13)	-62.6(15)	-50.2(25)	-53.4(21)
1	2	0	0	58.4(13)	60.30(98)	72.4(26)	59.4(12)
2	0	2	0	-32.5(83)	-29.90(18)	-25.9(16)	-25.44(27)
0	0	2	2	5.57(37)	4.29(12)	16.28(74)	8.67(20)
0	2	0	2	2.87(39)	2.16(13)	10.73(76)	5.82(24)
0	2	2	0	7.49(39)	4.69(15)	10.77(76)	6.06(23)
2	0	0	2	-39.64(87)	-36.88(17)	-23.5(17)	-30.45(27)
2	2	0	0	-25.23(91)	-14.93(25)	-11.0(18)	-12.03(25)
3	0	0	0	-148.4(44)	-183.89(87)	-231.2(87)	-168.5(13)
d_{rms}				30.9 cm^{-1}	133.2 cm^{-1}	61.0 cm^{-1}	210.9 cm^{-1}

^aFixed to $1/2 \omega_i$ in columns I and II, fixed to $1/2 \omega_i^{\text{scal}}$ according to Eq. (39) in columns III and IV.

as other examples in Table II. These discrepancies suggest that the quality of the *ab initio* MP2 (basis set 1) dipole moment surface is not adequate to describe the intensities in the fundamental region of CDBrClF. This deficiency can be understood by the coordinate dependence of the dipole moment μ_b which changes sign near $0.5 \leq q_f \leq 1$, at an energy which corresponds roughly to the region of $N=1$. Since the intensities depend on the dipole moment derivative, the quality of the dipole moment surface is very sensitive to errors in this region. Representative two-dimensional cuts through the 4D dipole moment surface are shown in (EPAPS) (Ref. 25) (Fig. A.8) for the components μ_a , μ_b , and μ_c .

We have also analyzed the *ab initio* potential energy surface in terms of a Taylor series expansion

$$V(q_s, q_f, q_a, q_b)/hc = \sum_{i,j,k,l} C_{s^i f j a^k b^l} q_s^i q_f^j q_a^k q_b^l, \quad (40)$$

where the coefficients C_{ii} were fixed to the value of the harmonic force constants of mode i . In agreement with earlier observations^{12,41,49} many terms are needed for a moderately accurate representation of the potential energy surface.

Table IX shows some of the most important expansion coefficients. The expansion coefficients $C_{s^i f j a^k b^l}$ are collected in EPAPS (Ref. 25); the pure *ab initio* MP2 data with parameters adjustment to fourth order up to 6000 cm^{-1} (Table A.1) and up to 15 000 cm^{-1} (Table A.2); the scaled MP2 data with parameters adjustment to fourth order up to 6000 cm^{-1} (Table A.3) and up to 15 000 cm^{-1} (Table A.4). The difference of the expansion coefficients from MP2 and scaled MP2 data can be understood because of the different coordinate ranges of the potential energy surface involved for the Taylor expansion, in spite of identical limiting poten-

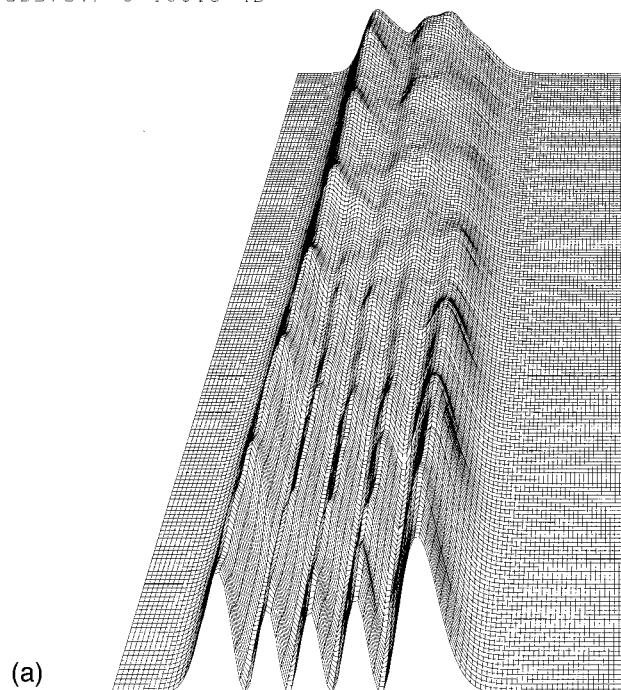
tial energies. No simple quantitative relation between effective parameters and corresponding Taylor expansion coefficients of the potential is observed, not even for those coefficients (such as the cubic potential constants) that are formally related to the effective parameters by low order perturbation theory. In other cases there are also other contributions of considerable magnitude, e.g., $C_{s^0 f^2 a^1 b^0}$, which contribute to effective parameters (such as x'_{fa}, k'_{saf}). Quite generally there is *no simple* relationship between potential constants and effective parameters.^{4,8,12,41,49,50} The existence of such simple relationships is still widely accepted and our results provide further evidence against it.

VII. TIME DEPENDENT DYNAMICS

Figure 11 shows a probability density (“wave packet”) [see Eq. (22)] in the coordinate q_s for an initial state $|v_s\rangle = |4\rangle$ and all other modes initially in the ground state. The time evolution shows a relaxation of the wave packet on the 100 fs time scale by an almost complete loss of its node structure. This is quite characteristic of the isolated CH chromophore⁴² and is an indication of a relaxation to a microcanonical equilibrium on this time scale.

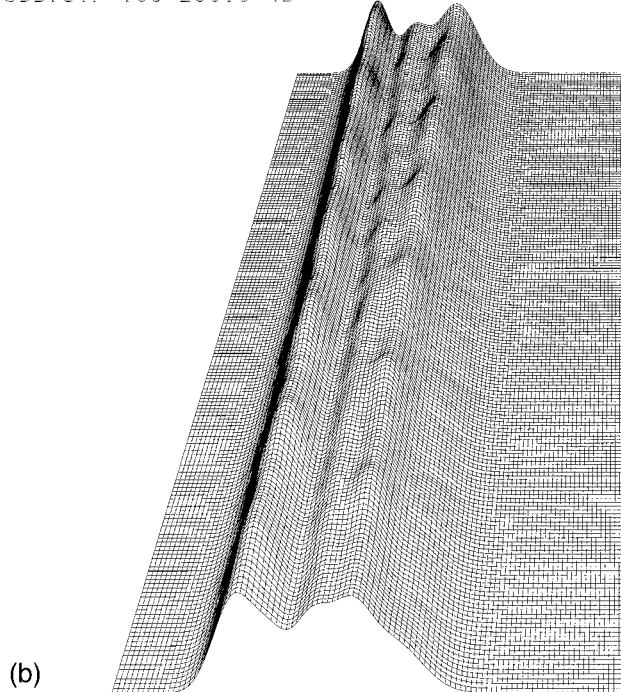
Figure 12 shows the “arrival” of the excitation in the coordinate q_f for the same initial state and time range as in Fig. 11. Initially, the ground state in q_f coordinate space is approximately a Gaussian distribution which broadens and almost fills the complete accessible q_f coordinate space after about 100 fs [Fig. 12(a)] with very weak indications of structure at later times [Fig. 12(b)]. A somewhat more coarse grained description is provided by the populations of the basis states. Figure 13 shows the time evolution of some

CDBrClF 0-100fs 4D



(a)

CDBrClF 100-200fs 4D



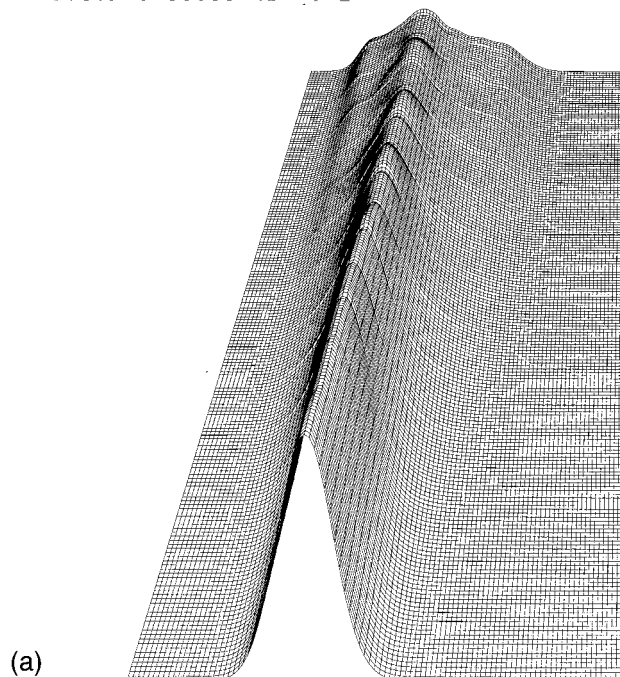
(b)

FIG. 11. (a) and (b) Time-dependent probability density $P(q_s, t)$ from 0 to 100 fs (top) and 100 to 200 fs (bottom) with $v_s=4$ as initial state. The reduced normal coordinate range for q_s is from -5 to $+9$ (which corresponds to $-61 \leq Q_s/(u^{1/2} \text{ pm}) \leq 110$). Time axis is from front to back in spacings of 0.05 fs.

effective Hamiltonian basis states of the polyad $N=4$ coupled by the parameters given in Table VIII. We observe a fast relaxation of population out of the initial $|4, 0, 0, 0\rangle$ state with almost no recurrence at later times within 1 ps. This behavior is more pronounced in the polyad $N=5$ due to a higher number of coupled states (Fig. 14).

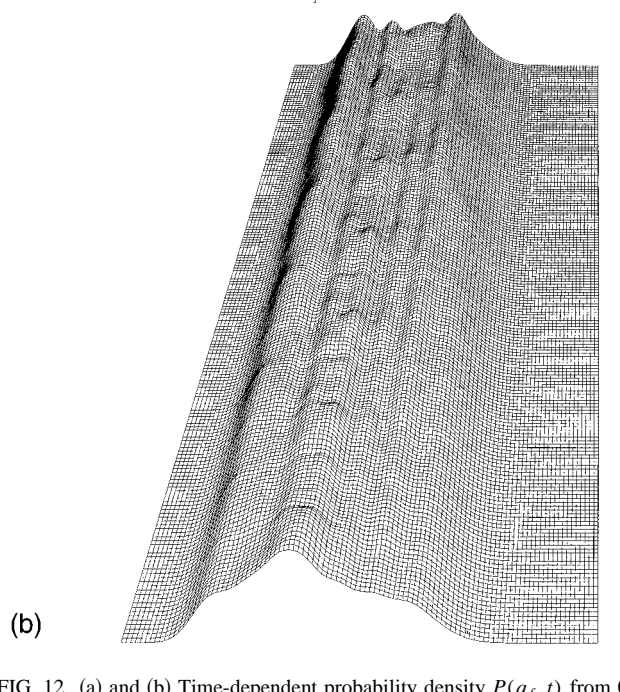
Time-dependent observables offer the possibility of

CDBrClF 0-100fs 4D qf-2



(a)

CDBrClF 100-200fs 4D qf-2



(b)

FIG. 12. (a) and (b) Time-dependent probability density $P(q_f, t)$ from 0 to 100 fs (top) and 100 to 200 fs (bottom) with $v_s=4$ as initial state. The reduced normal coordinate range for q_f is from -5 to $+9$ (which corresponds to $-88 \leq Q_f/(u^{1/2} \text{ pm}) \leq 158$); time axis is from front to back in spacings of 0.05 fs.

gaining additional insight into intramolecular vibrational redistribution processes. A clear conceptual background for the description as well as the interpretation of intramolecular vibrational (rotational) redistribution (IVR) processes in polyatomic molecules has been formulated quite recently (Ref. 14, and references therein). Here we focus on the zero-field dynamics obtained by the time-evolution of some selected

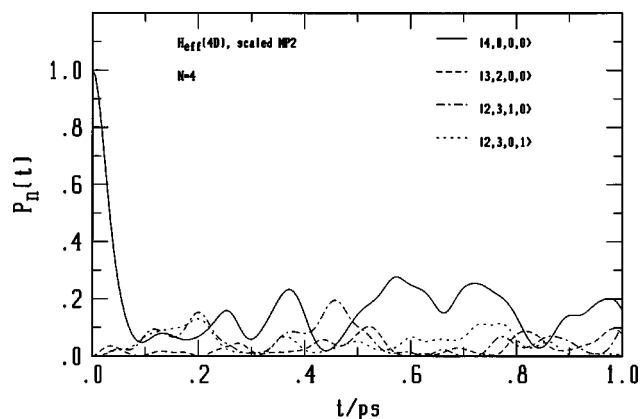


FIG. 13. Time-dependent population $P_n(t)$ for some selected states $|v_s, v_f, v_a, v_b\rangle$ in the $N=4$ polyad with $|4, 0, 0, 0\rangle$ (solid line), $|3, 2, 0, 0\rangle$ (dashed), $|2, 3, 1, 0\rangle$ (dashed-dotted), $|2, 3, 0, 1\rangle$ (dotted) from 0 to 1 ps in the 4D effective Hamiltonian model with the scaled MP2 surface.

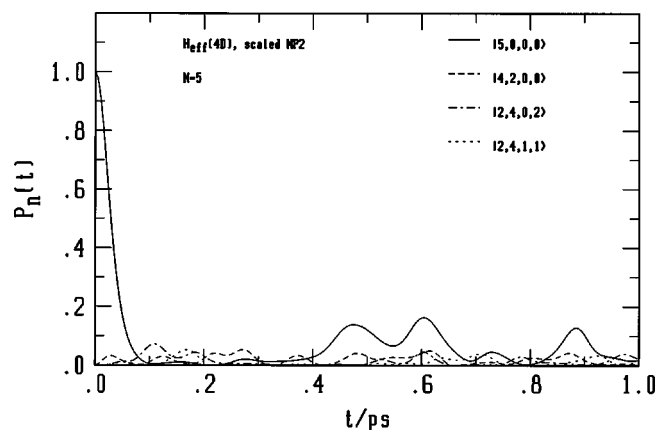


FIG. 14. Time-dependent population $P_n(t)$ for some selected states $|v_s, v_f, v_a, v_b\rangle$ in the $N=5$ polyad with $|5, 0, 0, 0\rangle$ (solid line), $|4, 2, 0, 0\rangle$ (dashed), $|2, 4, 0, 2\rangle$ (dashed-dotted), $|2, 4, 1, 1\rangle$ (dotted) from 0 to 1 ps in the 4D effective Hamiltonian model with the scaled MP2 surface.

initial state (e.g., some pure stretching state of the isolated CH- or CF-chromophore).^{27,42}

We can look at the microcanonical fine-grained Pauli entropy, $S_f(t)$, in the effective Hamiltonian basis,^{4,40,42}

$$S_f(t) = -k \sum_j p_j(t) \cdot \ln[p_j(t)], \quad (41)$$

where summation of the population $p_j(t)$ is performed over states in a polyad N , which defines the microcanonical ensemble. Another observable, the coarse-grained entropy, $S_Q(t)$, is closely related to $S_f(t)$ (see Ref. 4, and references therein). $S_Q(t)$ is a weighted average of the averaged sublevel populations where a sublevel consists of states with the same number of stretching quanta v_s or v_f . The weighting function $g(v_s)$ is here the degeneracy of a given sublevel v_s for a given N ,

$$S_Q(t) = -k \sum_{v_s=0}^N g(v_s) \cdot \langle p_{v_s}(t) \rangle \cdot \ln[\langle p_{v_s}(t) \rangle], \quad (42)$$

$$\langle p_{v_s}(t) \rangle = \sum_{j=1}^{g(v_s)} P_{j(v_s)}(t) / g(v_s), \quad (43)$$

with

$$g(v_s) = (N - v_s + 1) \cdot (2 \cdot (N - v_s + 1) - 1) \quad (44)$$

for integer N . Figure 15 shows the time dependent entropy for the polyads $N=4$ and 5 in the effective Hamiltonian basis.

The microcanonical ensemble is defined as the levels within a polyad. Thus, for $N=4$ we have 95 states [see Eq. (16)]. Within about 100 fs the maximum value of S_f is not reached, which may indicate an approximate symmetry. The number of states with v_b odd (v_b corresponds approximately to the a'' ("out-of-plane") vibration, see Fig. 3) for given integer N is given by

$$g(v_b^{\text{odd}}) = N(N+1)(N+2)/3, \quad (45)$$

and thus, the maximal value of $S/S_{\text{max}} \approx 0.81$ ($N=4$) or 0.84 ($N=5$), which is well reached on a very short time scale. In CDBrCIF we may thus assume the limiting case of near conservation of a formal a' symmetry, as already discussed in Ref. 14 for CHBrCIF [see Fig. 7(b) therein].

The partial equilibration implied by the fast rise of $S(t)$ to S_{max} on the 100 fs time scale does not include the remaining five vibrational modes. Thus beyond the approximate C_s symmetry of the dynamics on short time scales, there is also a strong separation between the time scale⁵¹ for the redistribution in the subsystem of four strongly coupled high frequency modes and the time scale for the redistribution between this subsystem and the remaining vibrational modes of lower frequency in CDBrCIF. The degree of the restricted equipartition on short time scales can be related to the relative numbers of states within the polyad, i.e., W_N^{4D} in Eq. (16) compared to $W_N^{9D} = W(E_2) - W(E_1)$, where $W(E)$ is the total number of vibrational states up to energy E . If one calculates W_N^{9D} from a separable anharmonic approximate vibrational model as customary in unimolecular reactions⁵² one finds $W_4^{9D} \approx 5.6 \cdot 10^5$ (compared to $W_4^{4D} = 95$) and $W_5^{9D} \approx 2.7 \cdot 10^6$ (compared to $W_5^{4D} = 161$). A more accurate calculation which convolutes the density from the Hamiltonian in the 4D subspace with an anharmonically counted density in the other modes would give a number of states $W_N^{9D, \text{conv}}$ similar to the approximate result. For example $S_{\text{max}}^{4D}(N=4)/k \approx 4.55$ and $S_{\text{max}}^{4D}(N=5)/k \approx 5.08$, whereas $S_{\text{max}}^{9D}(N=4)/k \approx 13.24$ and $S_{\text{max}}^{9D}(N=5)/k \approx 14.81$, which are substantially larger than the 4D values with or without the approximate dynamical symmetry.

VIII. CONCLUSIONS

We may summarize some of the main conclusions from the present study of D-isotope effects on IVR in the chiral molecule CDBrCIF.

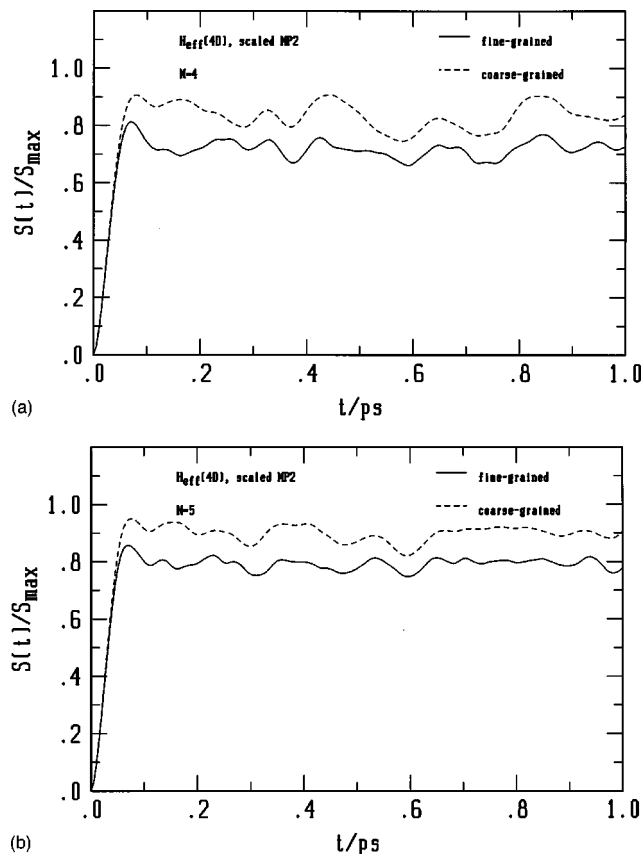


FIG. 15. (a) and (b) Time-dependent fine-grained [$S_f(t)$, solid line] and coarse-grained [$S_Q(t)$, dashed line] entropy from 0 to 1 ps within the 4D effective Hamiltonian model with the scaled MP2 surface for polyad $N=4$ (top) and $N=5$ (bottom); $S_{\max}/k = \ln 95 \approx 4.55$ ($N=4$) and $\ln 161 \approx 5.08$ ($N=5$).

- (i) The analysis of the complete spectra from the FIR to the NIR obtained here for the first time for CDBrCIF show overall good qualitative agreement with *ab initio* predictions. The experimentally scaled potentials indeed give a fairly quantitative description. This general conclusion is of relevance for current efforts in predicting potentials for coupled anharmonic vibrations by advanced *ab initio* techniques.⁵³
- (ii) The analysis of the complex Fermi resonance structure in the overtone spectrum using 3D and 4D effective Hamiltonians as well as complete variational 4D molecular adjusted model hamiltonians show as a new phenomenon an important Fermi-resonance coupling between the C–D stretching mode $\nu_s = \nu_1$ and the C–F stretching mode $\nu_f = \nu_4$, which contains some appreciable CD bending character. The effective coupling constant for this Fermi resonance is $k'_{sff} \approx 50 \pm 10 \text{ cm}^{-1}$.
- (iii) The other Fermi resonance CD stretch–bend couplings k'_{saa} and k'_{sbb} , as well as the “chiral” symmetry breaking coupling constants k'_{sfa} , k'_{sfb} and k'_{sab} are all of large absolute magnitude, also between 20 and 90 cm^{-1} . However, the last two constants are not currently very well constrained by experiment.
- (iv) These findings have consequences for the time evolution of populations, wave packets and intramolecular

Pauli-type entropy, which all show partial intramolecular equilibration for the strongly coupled modes on a very short time scale of 100 fs. On the other hand there is a strong separation from the much longer time scale of coupling these four modes to the remaining five vibrational degrees and the rotational degrees of freedom for which a bound can be estimated from smaller observed resonance splittings and bandwidths in the overtone region.

- (v) The effective short time IVR processes in CDBrCIF are thus quite different from those in CHBrCIF, where the strong couplings are restricted to the subset of three modes, at least at low energies.¹⁴ This restriction arises not because of the smallness of k'_{sff} in CHBrCIF but rather because of the resonance mismatch between the CH stretching mode and CF stretching overtone. *Ab initio* calculations on CHBrCIF indicate that k'_{sff} is about $40\text{--}50 \text{ cm}^{-1}$ which would lead to efficient IVR only in very high polyads (N around 8).

CDBrCIF is thus a molecule in which fast IVR occurs between CD and CF stretching modes with these two substituents in α position at the carbon atom. This may be compared with the recently established Fermi resonance between CH stretching and CF stretching modes of substituents in (α , β) positions in CF_3CHFI (Ref. 54) and the quartic 1:1 resonance of CH and OH stretching modes in (α , β) positions in CHD_2OH .^{2,50} The CD stretching–CF stretching Fermi resonance was previously surmised during the analysis of CD stretching spectra in CDF_3 ,⁵⁵ but could not be fully analyzed in terms of the relevant Fermi resonance couplings at the time.

CDBrCIF is of particular interest for infrared laser chemistry as three fundamentals of the Fermi resonance subsystem fall into either the $10.4 \mu\text{m}$ or the $9.4 \mu\text{m}$ band of the CO_2 -laser emission, i.e., vibrational excitation and unimolecular laser induced reaction may show interesting effects.^{56,44} As a chiral molecule accessible to ultrahigh resolution spectroscopy using CW- CO_2 laser lines, CDBrCIF may also be of interest in relation to fundamental questions related to parity violating forces and the understanding of chirality in general.^{57–61} These results are of interest for IR multiphoton excitation induced racemization kinetics in relation to parity violation.^{57,61} It will be interesting to investigate the consequences of chirality and symmetry in relation with the quantum dynamics during coherent excitation.⁶²

ACKNOWLEDGMENTS

Help from and discussions with David Luckhaus and Greg Tschumper are gratefully acknowledged. Our work is supported financially by the Schweizerische Nationalfonds and ETH Zürich.

- ¹C. S. Parmenter, J. Chem. Soc., Faraday Discuss. **75**, 7 (1983).
- ²L. Lubich, O. V. Boyarkin, R. D. F. Settle, D. S. Perry, and T. R. Rizzo, J. Chem. Soc., Faraday Discuss. **102**, 167 (1995), and discussion remarks by I. Mills (p. 244), M. Quack (pp. 245, 253).
- ³H.-R. Dübal and M. Quack, J. Chem. Phys. **81**, 3779 (1984).
- ⁴M. Quack, Annu. Rev. Phys. Chem. **41**, 839 (1990).
- ⁵*Femtosecond Chemistry*, edited by J. Manz and L. Woeste (Verlag Chemie, Weinheim, 1994), in *Proceedings of the Berlin Conference on Femtosecond Chemistry*, Berlin, March, 1993 (2 Volumes), pp. I–IX.
- ⁶M. Quack, *Femtosecond Chemistry*, edited by J. Manz and L. Woeste (Verlag Chemie, Weinheim, 1995), Chap. 27, pp. 781–818.
- ⁷R. Marquardt, M. Quack, J. Stohner, and E. Sutcliffe, J. Chem. Soc., Faraday Trans. 2 **82**, 1173 (1986).
- ⁸R. Marquardt and M. Quack, J. Chem. Phys. **95**, 4854 (1991).
- ⁹M. Quack and W. Kutzelnigg, Ber. Bunsenges. Phys. Chem. **99**, 231 (1995).
- ¹⁰M. Quack, Jerus. Symp. **24**, 47 (1991).
- ¹¹A. Beil, D. Luckhaus, and M. Quack, in *Thirteenth Colloquium on High Resolution Molecular Spectroscopy*, edited by E. Cané, T. F., and E. Venturi (Riccione, Italy, 1993); Cooperativa Universitaria Studio e Lavoro a r. l., Bologna, poster B 23.
- ¹²A. Beil, D. Luckhaus, and M. Quack, Ber. Bunsenges. Phys. Chem. **100**, 1853 (1996).
- ¹³A. Beil, D. Luckhaus, R. Marquardt, and M. Quack, J. Chem. Soc., Faraday Discuss. **99**, 49 (1994).
- ¹⁴A. Beil, D. Luckhaus, M. Quack, and J. Stohner, Ber. Bunsenges. Phys. Chem. **101**, 311 (1997).
- ¹⁵A. Beil, Dissertation No. 11744, ETH Zürich, 1996.
- ¹⁶A. Bauder, A. Beil, D. Luckhaus, F. Müller, and M. Quack, J. Chem. Phys. **106**, 7558 (1997).
- ¹⁷M. Diem and D. F. Burow, J. Chem. Phys. **64**, 5179 (1976).
- ¹⁸M. Diem, L. Nafie, and D. Burow, J. Mol. Spectrosc. **71**, 446 (1978).
- ¹⁹M. Diem and D. F. Burow, J. Phys. Chem. **81**, 476 (1977).
- ²⁰C. Marcott, T. R. Faulkner, A. Moscovitz, and J. Overend, J. Am. Chem. Soc. **99**, 8169 (1977).
- ²¹P. Prasad and D. Burow, J. Am. Chem. Soc. **101**, 806 (1979).
- ²²D. Madsen, R. Pearman, and M. Gruebele, J. Chem. Phys. **106**, 5874 (1997).
- ²³T. Doyle, Ph.D. thesis, Polytechnic University, Brooklyn, New York, 1989.
- ²⁴T. R. Doyle and O. Vogl, J. Am. Chem. Soc. **111**, 8510 (1989).
- ²⁵See EPAPS Document No. E-JCPSA6-113-020008 including the synthesis of Deuterobromochlorofluoromethane CDBrClF (3 pages), 8 figures (8 pages, high resolution spectra A.1: fundamental ν_7 ; A.2: fundamentals ν_6, ν_5 ; A.3: fundamental ν_1 ; A.4: survey of $N=5/2$; A.5: survey of $N=7/2$; A.6: survey of $N=4$; A.7: surveys of $N=9/2$ and $N=5$; A.8: 2D cuts of the *ab initio* 4D dipole moment surface²⁵ μ_a, μ_b, μ_c) and 5 tables (15 pages, A.1: fourth order Taylor expansion coefficients $C_{s'jla'kb'l}$ of the MP2 surface up to 6000 cm⁻¹; A.2: fifth order Taylor expansion coefficients $C_{s'jla'kb'l}$ of the MP2 surface up to 15 000 cm⁻¹; A.3: same as A.1 but scaled MP2 surface; A.4: same as A.2 but scaled MP2 surface; A.5: observed absolute and relative, scaled *ab initio* absolute and relative and effective scaled *ab initio* relative intensities for 4D effective transition wave numbers). This document may be retrieved via the EPAPS homepage (<http://www.aip.org/pubservs/epaps.html>) or from <ftp.aip.org> in the directory /epaps/. See the EPAPS homepage for more information.
- ²⁶K. v. Puttkamer and M. Quack, Mol. Phys. **62**, 1047 (1987).
- ²⁷M. Quack, J. Mol. Struct. **347**, 245 (1995).
- ²⁸I. Mills, T. Cvitaš, K. Homann, N. Kallay, and K. Kuchitsu, *Quantities, Units, and Symbols in Physical Chemistry*, 2nd ed. (Blackwell Scientific, Oxford, 1993).
- ²⁹T. H. Dunning, Jr., J. Chem. Phys. **53**, 2823 (1970).
- ³⁰T. H. Dunning, Jr. and P. J. Hay, *Modern Theoretical Chemistry*, edited by H. F. Schaefer (Plenum, New York, 1977), Vol. 3, Chap. 1, pp. 1–27.
- ³¹T. H. Dunning, Jr., J. Chem. Phys. **66**, 1382 (1977).
- ³²M. J. Frisch, G. W. Trucks, M. Head-Gordon, P. M. W. Gill, M. W. Wong, J. B. Foresman, B. G. Johnson, H. B. Schlegel, M. A. Robb, E. S. Replogle, R. Gomperts, J. L. Andres, K. Ragavachari, J. S. Binkley, C. Gonzales, R. L. Martin, D. J. Fox, D. J. Defrees, J. Baker, J. J. P. Stewart, and J. A. Pople, GAUSSIAN94, Gaussian, Inc., Pittsburgh, Pennsylvania, 1994.
- ³³R. Meyer, J. Chem. Phys. **52**, 2053 (1970).
- ³⁴D. Luckhaus and M. Quack, Chem. Phys. Lett. **190**, 581 (1992).
- ³⁵D. Luckhaus, Ber. Bunsenges. Phys. Chem. **101**, 346 (1997); J. Chem. Phys. **106**, 8409 (1997).
- ³⁶Z. Bačić and J. C. Light, Annu. Rev. Phys. Chem. **40**, 469 (1998).
- ³⁷H.-R. Dübal and M. Quack, Mol. Phys. **53**, 257 (1984).
- ³⁸A. Amrein, H.-R. Dübal, and M. Quack, Mol. Phys. **56**, 727 (1985).
- ³⁹M. Quack and H. J. Thöne, Ber. Bunsenges. Phys. Chem. **87**, 582 (1983).
- ⁴⁰M. Quack and J. Stohner, J. Phys. Chem. **97**, 12574 (1993).
- ⁴¹M. Lewerenz and M. Quack, J. Chem. Phys. **88**, 5408 (1988).
- ⁴²D. Luckhaus, M. Quack, and J. Stohner, Chem. Phys. Lett. **212**, 434 (1993).
- ⁴³M. Quack, Adv. Chem. Phys. **50**, 395 (1982).
- ⁴⁴M. Quack, in *Encyclopedia of Computational Chemistry*, edited by P. v. Ragué Schleyer, N. Allinger, T. Clark, J. Gasteiger, P. A. Kollman, H. F. Schaefer III, and P. R. Schreiner, (Wiley, New York, 1998), pp. 1775–1791.
- ⁴⁵M. P. Barchewitz, *Spectroscopie Infrarouge I, Vibrations Moléculaires* (Gauthier-Villars, Paris, 1961).
- ⁴⁶G. Amat, H. H. Nielsen, and G. Tarrago, *Rotation-Vibration of Polyatomic Molecules* (Marcel Dekker, New York, 1971).
- ⁴⁷C. Cohen-Tannoudji, B. Diu, and F. Laloë, *Mécanique Quantique* (Hermann, Paris, 1977), Vol. 1.
- ⁴⁸M. Hippler and M. Quack, J. Chem. Phys. **104**, 7426 (1996).
- ⁴⁹H.-R. Dübal, T.-K. Ha, M. Lewerenz, and M. Quack, J. Chem. Phys. **91**, 6698 (1989).
- ⁵⁰M. Quack and M. Willeke, J. Chem. Phys. **110**, 11958 (1999).
- ⁵¹J. Segall, R. N. Zare, H. R. Dübal, M. Lewerenz, and M. Quack, J. Chem. Phys. **86**, 634 (1987).
- ⁵²M. Quack and J. Troe, in *Encyclopedia of Computational Chemistry*, edited by P. v. Ragué Schleyer, N. Allinger, T. Clark, J. Gasteiger, P. A. Kollman, H. F. Schaefer III, and P. R. Schreiner, (Wiley, New York, 1998), pp. 2708–2726.
- ⁵³J. D. Goddard, H. F. Schaefer, Y. Osamura, and Y. Yamaguchi, *A New Dimension to Quantum Chemistry: Analytic Derivative Methods in Ab Initio Molecular Electronic Structure Theory* (Oxford University Press, New York, 1994).
- ⁵⁴J. Pochert and M. Quack, Mol. Phys. **95**, 1055 (1998); J. Pochert, M. Quack, J. Stohner, and M. Willeke, J. Chem. Phys. **113**, 2719 (2000), following paper.
- ⁵⁵H.-R. Dübal, M. Lewerenz, and M. Quack, J. Chem. Phys. **85**, 34 (1986).
- ⁵⁶M. Quack, Infrared Phys. Technol. **36**, 365 (1995).
- ⁵⁷M. Quack, Angew. Chem. Int. Ed. Engl. **28**, 571 (1989); Nova Acta Leopold. **NF81**, 137 (1999).
- ⁵⁸C. Daussey, T. Marrel, A. Amy-Klein, C. Nguyen, C. Bordé, and C. Charbonnet, Phys. Rev. Lett. **83**, 1554 (1999).
- ⁵⁹M. Quack and J. Stohner, Phys. Rev. Lett. **84**, 3807 (2000).
- ⁶⁰M. Quack and J. Stohner, Z. Phys. Chem. (Munich) **214**, 675 (2000).
- ⁶¹M. Quack, Infrared Phys. **29**, 441 (1989).
- ⁶²O. Monti, M. Quack, and J. Stohner (in preparation).